AD-A160 921 ASYMPTOTIC FIELDS IN STEADY CRACK GROWTH WITH LINEAR STRAIN-HARDENING(U) HARVARD UNIV CAMBRIDGE MA DIV OF APPLIED SCIENCES P P CASTANEDA AUG 85 MECH-69 1/1

UNCLASSIFIED N00014-84-K-0510 F/G 20/11 NL

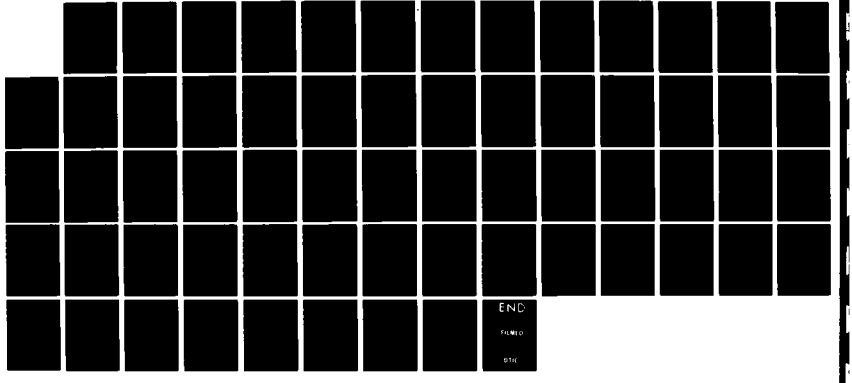

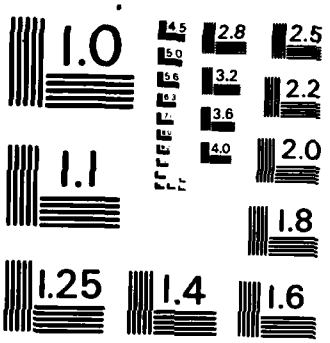

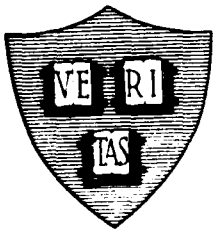

MECH-69

ASYMPTOTIC FIELDS IN STEADY CRACK GROWTH WITH LINEAR STRAIN-HARDENING

P. Ponte Castañeda

N00014-84-K-0510

Division of Applied Sciences
HARVARD UNIVERSITY
Cambridge, Massachusetts 02138

August 1985

ASYMPTOTIC FIELDS IN STEADY CRACK GROWTH WITH LINEAR STRAIN-HARDENING

P. Ponte Castañeda

Division of Applied Sciences
Harvard University
Cambridge, Massachusetts 02138

Abstract

The asymptotic stress and velocity fields of a crack propagating steadily and quasi-statically into an elastic-plastic material are presented. The material is characterised by J_2 flow theory with linear strain-hardening. The possibility of reloading on the crack flanks is taken into account. The cases of anti-plane strain (mode III), plane strain (modes I and II), and plane stress (modes I and II) are considered. Numerical results are given for the strength of the singularity and for the distribution of the stress and velocity fields in the plastic loading, elastic unloading and plastic reloading regions, as functions of the strain-hardening parameter. An attempt is made to make a connection with the perfectly-plastic solutions in the limit of vanishing strain-hardening.

1. Introduction

Knowledge of the stress and deformation fields near the tip of an advancing crack is central to the continued development of engineering fracture mechanics, and important advances have been made in recent years. Under the assumption of quasi-static growth and small-strain ideal elasto-plasticity, rigorous asymptotic solutions have been found in anti-plane strain by Chitaley and McClintock (1971); in plane strain by Slepyan (1974), Gao

(1980), Rice *et al.* (1980), and Drugan *et al* . (1982); and in plane-stress mode II by Ponte (1985a). In addition, a general discussion of the subject is found in Rice (1982).

The corresponding work for hardening elastic-plastic solids is at a less developed stage. For linear-hardening materials Amazigo and Hutchinson (1977) (referred to as AH in the sequel) produced steady-state asymptotic solutions using Mises flow theory for plane-strain and plane-stress mode I, and for anti-plane strain. These solutions, however, neglected the possibility of reverse plastic flow on the crack flanks which is known to occur in the elastic-perfectly plastic solutions mentioned above. In a recent publication Zhang *et al.* (1983) included reloading (as well as a Bauschinger effect) in their solution of the plane-strain mode I problem.

Further work on the hardening elastic-plastic steadily moving crack include publications by Slepyan (1973) who studied a mode III crack propagating in a linear-hardening J_2-deformation theory material, Lo and Pierce (1981) who considered a mode III crack moving in a linear-hardening corner-theory material, Gao *et al.* (1983) who investigated a mode III crack propagating in a power-hardening J_2-flow theory material, and Ponte (1985b) who studied the mode I crack propagating in a linear-hardening J_2-deformation theory material.

In this work we will include the possibility of reloading on the crack flanks of the linear-hardening J_2-flow theory problem. We will consider plane strain and plane stress (modes I and II), and anti-plane strain. Thus we will verify and expand the results of Zhang *et al.* for plane-strain mode I, we will correct the results of AH for plane-stress mode I and mode III, and we will produce new results for plane-strain and plane-stress mode II.

We propose to use a simple scheme that can be implemented numerically in a straightforward manner. Thus we formulate the problem in terms of a system of first order ODE's in the angular variations of the non-zero components of the stress tensor and the velocity vector instead of a single higher order equation in the stress function as was done

by AH. This procedure has the advantage that it can directly make use of well-developed Runge-Kutta integrators, and also that the boundary and continuity conditions are simplest in form.

In our numerical solutions we will go to very low values of the hardening parameter in order to try to make a connection with the perfectly-plastic problem. However, the work of Dunayevsky and Achenbach (1982) suggests that the region of validity of the power singularity solution to the linear-hardening problem vanishes in the limit of zero strain-hardening. Thus it is not clear whether the limiting solutions to the linear-hardening problem can in fact be related to the the perfectly-plastic solutions. Here, we will address these and related questions.

2. Anti-plane strain (mode III)

2.1 *Governing equations.*

With reference to Figure 2.1, let x_i (i = 1,2,3) be a Cartesian coordinate system of fixed orientation travelling with the crack tip such that the x_3-axis coincides with the straight crack front. Also let $\mathbf{e}_i$ be the unit vector corresponding to the x_i direction. Similarly, let r, θ be polar coordinates corresponding to x_α (α = 1,2) and $\mathbf{e}_r$, $\mathbf{e}_\theta$ be the corresponding unit vectors. The crack tip moves with velocity $\mathbf{V} = V\mathbf{e}_1$ with respect to the stationary coordinate system X_i. In our steady-state analysis the crack tip speed V is constant so that the material derivative is given by

$$(\,)^{\cdot} = -V(\,)_{,1} \tag{2.1}$$

The non-zero stresses are $\tau_\alpha = \sigma_{\alpha 3}$, and the only non-zero velocity component is v_3. Because it turns out to be simpler from an algebraic point of view, we choose to use the polar components of the stress vector $\boldsymbol{\tau}$ so that τ_r, τ_θ, and v_3 are the three variables of this problem. Then the equilibrium equation is

$$(r\tau_r)_{,r} + \tau_{\theta,\theta} = 0 \tag{2.2}$$

For our bilinear flow theory material the stress-strain relation is

$$2G\mathbf{D} = \mathbf{T} + (\underline{\alpha}^{-1} - 1)\,(\tau_e^{\cdot}/\,\tau_e)\,\boldsymbol{\tau} \tag{2.3}$$

where $\mathbf{D} = (1/2)\nabla v_3$ is the strain-rate vector, $\mathbf{T} = \boldsymbol{\tau}^{\cdot}$ is the stress-rate vector, $\tau_e = |\boldsymbol{\tau}|$ is the effective stress, and $\underline{\alpha}$ is either α for loading ($\tau_e^{\cdot} \geq 0$), or unity for unloading ($\tau_e^{\cdot} < 0$), where $\alpha = G_t/G$, the ratio of the tangent modulus to the elastic modulus in shear (Fig. 2.1), is a measure of the hardening.

It can be seen that (2.2) and (2.3) form a system of three first order PDE's in the two stress components and the single velocity component. Even though some of the equations are nonlinear (namely the constitutive equations), all three equations are homogeneous in the independent variables, which suggests that we look for solutions of the form

$$\begin{aligned} &\tau_r(r,\theta) = \tau_o\, y_1(\theta)\, r^s \qquad \tau_\theta(r,\theta) = \tau_o\, y_2(\theta)\, r^s \\ &v_3(r,\theta) = V\,(\tau_o/G)\, y_3(\theta)\, r^s/s \end{aligned} \tag{2.4}$$

where r is nondimensionalised with respect to some measure of the plastic zone size, R. Putting these into (2.2) and (2.3) we are left with a system of three first order ODE's in the vector $\mathbf{y} = (y_1, y_2, y_3)$

$$\mathbf{y}'(\theta) = \mathbf{f}(\theta, \mathbf{y}; s, \underline{\alpha}) \tag{2.5}$$

where the the components of $\mathbf{f}$ are given in Appendix A and depend on whether loading or unloading occurs through the parameter

$$\begin{aligned} \underline{\alpha} &= \alpha \quad \text{if } \phi^{\cdot} \geq 0 \\ &= 1 \quad \text{if } \phi^{\cdot} < 0 \end{aligned} \tag{2.6}$$

where

$$\phi^{\cdot}(\theta) = r\,\tau_e^{\cdot}/\,\tau_e = -s\cos\theta + \sin\theta\,[y_e'(\theta)\,/\,y_e(\theta)] \tag{2.7}$$

$$\tau_e = \tau_o\, y_e(\theta)\, r^s \tag{2.8}$$

and s is some as yet unknown function of α.

2.2 *Boundary conditions*

Anti-plane symmetry ahead of the crack tip reduces to the two independent conditions

$$y_1(0) = y_3(0) = 0 \tag{2.9}$$

and vanishing traction on the crack face requires that

$$y_2(\pi) = 0 \tag{2.10}$$

Thus we have three homogeneous boundary conditions to be satisfied by (2.5). It follows that the strength of the singularity, s, will be determined as an eigenvalue of the problem, and an amplitude factor corresponding to the stress intensity factor in the elastic problem will be left undetermined in this asymptotic solution. We can then initially set

$$y_2(0) = 1 \tag{2.11}$$

even though once we obtain a solution we will renormalise it such that

$$y_e(\theta_1) = 1 \tag{2.12}$$

where θ_1 is the unloading angle (to be defined in the next section).

2.3 *Loading history of a near-tip particle.*

Consider the state of stress of a particle P at a given distance $\bar{x}_2$ above the crack line as it moves past the crack tip (or, equivalently, as the crack tip moves past it) as depicted in Figure 2.2a. Note that we can describe the location of this particle by giving its x_1 coordinate, or, alternatively, by giving its angular coordinate $\bar{\theta} = \tan^{-1}(\bar{x}_2/x_1)$.

It is expected that the particle will experience plastic loading ahead of the crack, but then unload elastically for some critical value of $\bar{\theta}$, denoted θ_1, defining the location of the straight unloading boundary. This is seen to be consistent with the fact that in the elastic solution τ_e has a maximum for a value of $\bar{\theta}$ between zero and π.

For a hardening material ($0 < \alpha < 1$), a particle in the elastic unloading zone retains the plastic strain state it had when it unloaded. Thus it is expected that when the particle is

deep into the wake of the crack ($\bar{\theta} \to \pi$), its associated stress state will approach some non-vanishing wake level, τ^w. Plastic reloading takes place on the crack flank if the effective stress level, τ_e^w, associated with the wake stress state is greater than the effective stress level, $\tau_e^l = \tau_o\, y_e(\theta_1)\, (\bar{x}_2 / \sin\theta_1)^s$, that the particle had at unloading. Hence, it is expected that for some values of α, plastic reloading will start at some critical value of $\bar{\theta}$, denoted θ_2, defining the reloading angle.

2.4 *Continuity conditions*

We need to connect the solutions in the different regions through appropriate continuity conditions. Recalling that in this problem we have a third order system in the two stress components and the single velocity component, we require three independent continuity conditions in these three variables across each unloading and reloading boundary.

Let [ ] denote the jump in a quantity as θ increases infinitesimally. Then the traction component of the stress must be continuous

$$[\tau_\theta] = 0 \tag{2.13}$$

and the displacement field must be continuous

$$[u_3] = 0 \tag{2.14}$$

Also for a work-hardening material it is consistent with the plastic rule to assume that the plastic strain vector is continuous

$$[\boldsymbol{\gamma}^{pl}] = \mathbf{0} \tag{2.15}$$

It follows from (2.14) that

$$[\gamma_r] = [u_{3,r}] = 0 \tag{2.16}$$

This condition, together with (2.15) yields

$$[\gamma_r^{el}] = 0 \tag{2.17}$$

which in turn implies that

$$[\tau_r] = 0 \tag{2.18}$$

and also that

$$[\tau_e] = 0 \tag{2.19}$$

Similarly, it follows from (2.13) that

$$[\gamma_\theta^{el}] = 0 \tag{2.20}$$

and that

$$[\gamma_\theta] = 0 \tag{2.21}$$

Finally, note that the velocity is given by

$$v_3 = -Vu_{3,1} = -V(\cos\theta\, u_{3,r} - \sin\theta\, u_{3,\theta}) \tag{2.22}$$

so that it follows from strain continuity that the velocity field must also be continuous

$$[v_3] = 0 \tag{2.23}$$

Conditions (2.13), (2.18), and (2.23) are the three independent conditions needed, and they take the convenient form in terms of angular variations

$$[y_1] = [y_2] = [y_3] = 0 \tag{2.24}$$

In order to close the mathematical problem we need to specify the conditions for unloading and reloading which determine the angles θ_1 and θ_2.

Unloading occurs at θ_1 when the effective stress-rate of the particle vanishes, or (see (2.7)) when

$$\phi^{\cdot}(\theta_1) = 0 \tag{2.25}$$

Reloading occurs at θ_2 if the effective stress of the particle regains its unloading value, or (see (2.8)) if

$$y_e(\theta_1) / (\sin\theta_1)^s - y_e(\theta_2) / (\sin\theta_2)^s = 0 \tag{2.26}$$

2.5 *Numerical integration*

We need to solve the third order system (2.5) subject to the three boundary conditions (2.9) and (2.10), and the continuity conditions (2.24). We selected a Runge-Kutta-Verner fifth and sixth order scheme to perform the numerical integration.

We provide the initial values of the dependent variables $y_i(0)$ through (2.9) and (2.11), and we need to guess the value of s for a given α. We then integrate equations (2.5) to find the values of $y_i(\theta)$ for $0 < \theta < \pi$, keeping track of whether unloading or reloading occurs in order to make use of the appropriate value of $\underline{\alpha}$. Once we have the values of $y_i(\pi)$ we check to see whether $y_2(\pi)$ is zero, and we iterate in our guess for s until convergence is achieved.

Note, however, that we cannot use (2.5) to find numerically the values of $y_i'(0)$, but we can easily take the appropriate limits to find that

$$\begin{aligned} y_1'(0) &= (1-s^2/\alpha) \,/\, (1-s/\alpha) \\ y_2'(0) &= 0 \\ y_3'(0) &= -s^2/\alpha \end{aligned} \tag{2.27}$$

Similarly, equations (2.5) are numerically ill-conditioned at $\theta = \pi$, but we can integrate them out to $\theta = \pi - \varepsilon$, and make ε as small as needed to obtain accurate results. Since $y_2(\theta)$ is well behaved near $\theta = \pi$, this approximation presents no difficulties.

2.6 *Results.*

The results are summarised in Figures 2.3 through 2.6, and in Table 2.1. Figure 2.3 is a plot of the strength of the singularity, s, versus the square root of the hardening parameter, α. It is observed, as pointed out by AH, that $s \sim -\alpha^{1/2}$ for small α.

Table 2.1 presents values of s, θ_1 and θ_2 for values of α such that $10^{-6} \le \alpha \le 1$, and it also includes for comparison the values of s and θ_1 obtained by AH. It is found that reloading occurs for all values of α such that $0 < \alpha < \alpha^*$ where $0.05 < \alpha^* < 0.1$ (a more accurate determination of α^* is an expensive task not worth the investment at this time). See Figure 2.2b for a schematic depiction of the loading history of a fixed particle. For $\alpha^* < \alpha < 1$ our results agree with those of AH as expected. For $0 < \alpha < \alpha^*$ the appearance of the thin reloading sector affects rather weakly the values of s and θ_1. Finally, observe that as $\alpha \to 0$ the values of θ_1 and θ_2, though still far from the corresponding perfectly-

plastic values (19.69° and 179.63°) of Chitaley and McClintock (1971), do appear to have an appropriate trend.

Figure 2.4 shows plots of the particle effective stress (fixed x_2) for $0 < \theta < \pi$ for three values of α (0.75, 0.1, 0.001) corresponding to large, moderate and small strain-hardening. The result for large strain-hardening is actually quite close to the elastic result, and no reloading is necessary. As α becomes smaller, the stress level ahead of the crack ($0 < \theta < \theta_1$) approaches a flat distribution, and a tiny reloading zone appears on the crack flank.

Figure 2.5 presents plots of the angular (fixed $\underline{r}$) variations of the stresses and velocity for large, moderate and small strain-hardening. The curves corresponding to α = 0.75 are not very different from the elastic curves with the exception of $\bar{\tau}_r$ (and $\bar{\tau}_e$) which near $\theta = \pi$ suddenly become unbounded. For $\alpha = 0.1$ the angular variations of the stresses and velocity undergo significant changes, and for $\alpha = 0.001$ they start taking the general shape of the perfectly-plastic results which are depicted in Figure 2.6. This is a remarkable result: even though the radial dependence of the velocity of the small-α problem ($\underline{r}^s/s$) does not approach that of the perfectly-plastic problem ($\ln\underline{r}$), the factored-out angular variation of the velocity of the small-α problem does seem to approach the perfectly-plastic result.

3. Plane strain (mode I)

3.1 *Formulation.*

Here the non-zero stress components are $\sigma_{\alpha\beta}$ and σ_{33}, and the non-zero velocity components are v_α. Again for algebraic convenience we choose to use the cylindrical components of the stress tensor $\boldsymbol{\sigma}$ and of the velocity vector $\mathbf{v}$, so that $\sigma_{r\theta}$, σ_{rr}, $\sigma_{\theta\theta}$, σ_{33}, v_r, and v_θ are the six variables of this problem. Then equilibrium requires

$$(r\sigma_{rr})_{,r} + \sigma_{r\theta,\theta} - \sigma_{\theta\theta} = 0 \qquad (3.1)$$

$$(r\sigma_{r\theta})_{,r} + \sigma_{\theta\theta,\theta} + \sigma_{r\theta} = 0 \tag{3.2}$$

For a bilinear ($\alpha = E_t/E$) flow-theory material the stress-strain relation is

$$E\mathbf{D} = (1+\nu)\boldsymbol{\Sigma} - \nu\, \mathrm{Tr}(\boldsymbol{\Sigma})\, \mathbf{I} + (3/2)\,(\underline{\alpha}^{-1}-1)\,(\sigma_e^{\cdot}/\sigma_e)\,\mathbf{S} \tag{3.3}$$

where ν is Poisson's ratio, $\mathbf{I} = \mathbf{e}_i\mathbf{e}_i$ is the identity tensor, $\mathbf{D} = (1/2)[\nabla\mathbf{v}+(\nabla\mathbf{v})^t]$ is the strain-rate tensor, $\boldsymbol{\Sigma} = \boldsymbol{\sigma}^{\cdot}$ is the stress-rate tensor, $\mathbf{S} = \boldsymbol{\sigma} - (1/3)\,\mathrm{Tr}(\boldsymbol{\sigma})\,\mathbf{I}$ is the stress-deviator tensor, $\sigma_e = [(3/2)\mathbf{S}:\mathbf{S}]^{1/2}$ is the effective stress, and $\underline{\alpha}$ is either α for loading ($\sigma_e^{\cdot} \geq 0$), or unity for unloading ($\sigma_e^{\cdot} < 0$).

Note that there are four non-trivial equations in (3.3) (including the plane strain condition $D_{33} = 0$) which means that (3.1), (3.2), and (3.3) form a system of six first order PDE's in the six dependent variables of the problem identified above. As we found in mode III, all six equations are homogeneous in the independent variables which suggests that we look for solutions of the form

$$\begin{aligned} v_r(r,\theta) &= V\,(\tau_o/E)\,y_1(\theta)\,r^s/s \qquad & v_\theta(r,\theta) &= V\,(\tau_o/E)\,y_2(\theta)\,r^s/s \\ \sigma_{r\theta}(r,\theta) &= \tau_o\, y_3(\theta)\, r^s & \sigma_{rr}(r,\theta) &= \tau_o\, y_4(\theta)\, r^s \\ \sigma_{\theta\theta}(r,\theta) &= \tau_o\, y_5(\theta)\, r^s & \sigma_{33}(r,\theta) &= \tau_o\, y_6(\theta)\, r^s \end{aligned} \tag{3.4}$$

Putting these in equations (3.1) through (3.3) we are left with a system of six first order ODE's in the vector $\mathbf{y} = (y_1, y_2, \ldots, y_6)$

$$\mathbf{y}'(\theta) = \mathbf{f}(\theta, \mathbf{y}; s, \alpha, \nu) \tag{3.5}$$

where the components of $\mathbf{f}$ are given in Appendix A, and depend on whether loading or unloading occurs through the parameter

$$\begin{aligned} \underline{\alpha} &= \alpha \quad \text{if } \phi^{\cdot} \geq 0 \\ &= 1 \quad \text{if } \phi^{\cdot} < 0 \end{aligned} \tag{3.6}$$

where

$$\phi^{\cdot} = r\,\sigma_e^{\cdot}/\sigma_e = -s\cos\theta + \sin\theta\,(y_e'/y_e) \tag{3.7}$$

$$\sigma_e = \tau_o\, y_e(\theta)\, r^s \tag{3.8}$$

and s is some as yet unknown function of α and ν.

Mode I symmetry ahead of the crack tip requires the four independent conditions

$$y_2(0) = y_3(0) = y_4'(0) = y_6'(0) = 0 \tag{3.9}$$

and vanishing tractions on the crack faces requires that

$$y_3(\pi) = y_5(\pi) = 0 \tag{3.10}$$

Thus we have six homogeneous boundary conditions to be satisfied by equations (3.5). As before s will be determined as an eigenvalue of the problem for given α and ν, and we can arbitrarily pick the amplitude factor of the angular variations.

The same arguments used in the mode III problem can be repeated here, and they lead us to expect a similar near-tip loading history for this case.

We next use the same development as before to determine the continuity conditions across an elastic-plastic boundary (unloading or reloading).

The traction components of the stress tensor must be continuous

$$[\sigma_{r\theta}] = [\sigma_{\theta\theta}] = 0 \tag{3.11}$$

The displacement field must also be continuous

$$[u_r] = [u_\theta] = 0 \tag{3.12}$$

and it is consistent with the plastic rule to assume that the plastic strain tensor is continuous

$$[\varepsilon^{pl}] = \mathbf{0} \tag{3.13}$$

It follows from (3.12) and the plane strain condition that

$$[\varepsilon_{rr}] = [\varepsilon_{33}] = 0 \tag{3.14}$$

which together with (3.11) and (3.13) imply that

$$[\sigma_{rr}] = [\sigma_{33}] = 0 \tag{3.15}$$

and also that

$$[\sigma_e] = 0 \tag{3.16}$$

We can next show that all the strain components are continuous, and therefore that

$$[v_r] = [v_\theta] = 0 \tag{3.17}$$

Conditions (3.11), (3.15), and (3.17) are the six conditions needed, and in terms of the angular variations they take the convenient form

$$[y_1] = [y_2] = \ldots = [y_6] = 0 \tag{3.18}$$

To these conditions we must add an unloading condition which determines θ_1

$$\phi'(\theta_1) = 0 \tag{3.19}$$

and a reloading condition which determines θ_2

$$y_e(\theta_1) / (\sin\theta_1)^s - y_e(\theta_2) / (\sin\theta_2)^s = 0 \tag{3.20}$$

The numerical integration of equations (3.5) was performed using the same scheme used in the mode III problem. In order to get started we need to provide the values of $y(0)$, $y'(0)$ and s for given α and ν.

We have already seen in (3.9) that $y_2(0) = y_3(0) = 0$. If we now pick the normalisation $y_4(0) = 1$, and guess the values of $y_5(0)$ and s, we find using (3.5) that

$$\begin{aligned} y_1(0) &= -s\,\{y_4(0)/\alpha - \lambda[y_5(0) + y_6(0)]\} \\ y_6(0) &= \alpha\,\lambda[y_4(0) + y_5(0)] \end{aligned} \tag{3.21}$$

with $\lambda = \nu + (\alpha^{-1}-1)/2.$

Similarly, since $y_4'(0) = y_6'(0) = 0$, we can use (3.5) to find that

$$\begin{aligned} y_1'(0) &= y_5'(0) = 0 \\ y_2'(0) &= -y_1(0) - s^2\{y_5(0)/\alpha - \lambda[y_4(0)+y_6(0)]\} \\ y_3'(0) &= -(1+s)y_4(0) + y_5(0) \end{aligned} \tag{3.22}$$

We then integrate equations (3.5) to find the values of $y(\theta)$ for $0 < \theta < \pi$ keeping track of whether unloading or reloading occurs. Given the values of $y_3(\pi)$ and $y_5(\pi)$ we check to see whether they vanish, and iterate in our guesses for $y_5(0)$ and s until convergence is achieved. Once this is accomplished we renormalise our solutions such that $y_e(\theta_1) = 1$. Note that y_3 and y_5 are well behaved near $\theta = \pi$, so that even though (3.5) is numerically ill-conditioned at $\theta = \pi$, a procedure analogous to that used in the mode III case is appropriate.

3.2 *Results.*

In this case we produced results for $\nu = 1/3$ for several values of α. It was noted by AH that the dependence of s and of the angular variations of the stresses on ν is weak.

Figure 3.1 depicts a plot of s versus $\alpha^{1/2}$; for large strain-hardening it looks very much like the corresponding plot for anti-plane strain, but as α gets smaller the curve reverses curvature, and s does not seem to be approaching zero.

Table 3.1 shows values of s, θ_1 and θ_2 for $0.001 \leq \alpha \leq 1$, and it also includes for comparison the values of s and θ_1 obtained by AH ignoring reloading. We first note that our results agree very well with those reported by Zhang *el al.* (1983). It is found that reloading occurs for $0 < \alpha < \alpha^*$ where $0.2 < \alpha^* < 0.3$. See Fig. 2.2b for a pictorial representation of the loading history. In contrast with the mode III results, reloading here starts at higher strain-hardening ($\alpha^* \sim 0.3$), the width of the reloading sector is much larger (31.6° at $\alpha = 0.001$), and the values of s and θ_1 are significantly affected by reloading (s is weaker by 10%, and θ_1 is smaller by 14% at $\alpha = 0.01$). Note further that for $\alpha = 0.001$ the width of the elastic sector is only 1.35°, and still decreasing strongly. Finally, we should remark that the values of θ_1 and θ_2 do not appear to be approaching the corresponding perfectly-plastic values (123.1° and 160.4° for $\nu = 0.3$) of the solution of Drugan *et al.* (1982).

Figure 3.2 shows plots of the particle (fixed x_2) effective stress for $0 < \theta < \pi$ for large, moderate and small strain-hardening corresponding to values of α of 0.75, 0.1 and 0.001, respectively. For large strain-hardening small changes from the elastic solutions occur, and no reloading is necessary. For moderate strain-hardening well-defined changes take place: a smooth unloading (continuous $\sigma_e^{\cdot}$), and a sudden (discontinuous $\sigma_e^{\cdot}$) reloading are clearly observed. As we make α smaller, the elastic unloading sector virtually disappears, and even though the stress level ahead of the crack increases, it is still far from approaching a flat distribution corresponding to the perfectly-plastic yield condition.

Figure 3.3 presents plots of the angular (fixed r) variations of the stresses $\bar{\sigma}_{r\theta}$, $\bar{\sigma}_{rr}$, $\bar{\sigma}_{\theta\theta}$, $\bar{\sigma}_{33}$, and $\bar{\sigma}_e$ for large, moderate and small strain-hardening. The curves for $\alpha = 0.75$ are not very different from the elastic curves except that $\bar{\sigma}_{rr}$, $\bar{\sigma}_{33}$ and $\bar{\sigma}_e$ become unbounded near $\theta = \pi$. Figure 3.4 shows the angular variations of the Cartesian

components of the stress for $\alpha = 0.001$. It can be seen that the angular variations of the stresses seem to be approaching the general shape of the stresses in a Prandtl field. But for $\alpha = 0.001$ the agreement is still not very good; for instance $\bar{\sigma}_e(\theta)$ changes by 50% between zero and θ_1 instead of remaining constant throughout.

Figure 3.5 shows plots of the angular variations of the Cartesian components of the velocity for large, moderate and small strain-hardening ($\alpha = 0.75, 0.1, 0.01$). It is observed that, contrary to what happens in mode III, the angular variations of the velocity do not remain of the same order of magnitude as those of the stresses, and do not seem to be approaching a limit as $\alpha \to 0$. This is an understandable consequence of the fact that s does not vanish in the limit in this case.

4. Plane strain (mode II)

4.1 *Formulation.*

The formulation of this problem is identical to that of the mode I problem except for the boundary conditions ahead of the crack tip. Mode II symmetry requires the four independent conditions

$$y_1(0) = y_4(0) = y_5(0) = y_6(0) = 0 \tag{4.1}$$

It is convenient here to pick the normalisation $y_3(0) = 1$, and to guess the values of $y_2(0)$ and s. We can then use equations (3.5) to find that

$$\begin{aligned} y_1'(0) &= (1-s)\, y_2(0) - 2s^2 [(1+\nu) + (3/2)(\alpha^{-1}-1)]\, y_3(0) \\ y_2'(0) &= y_3'(0) = 0 \\ y_5'(0) &= -(s+2)\, y_3(0) \end{aligned} \tag{4.2}$$

plus two other more complicated equations for $y_4'(0)$ and $y_6'(0)$ which we will not write out in detail.

Given the values of y(0) and y'(0) we can start integrating equations (3.5) making use of the continuity conditions developed in Section 3 to connect regions of different physical behavior. As before we need to check whether $y_3(\pi)$ and $y_5(\pi)$ are zero, and to iterate in the guesses of s and $y_2(0)$ until convergence is achieved. When we are finished we renormalise the solution in the usual way such that $y_e(\theta_1) = 1$.

4.2 *Results.*

In this case we produced results for $\nu = 1/3$ for several values of α. Figure 4.1 shows a plot of s versus $\alpha^{1/2}$; it looks very much like the corresponding mode III plot, and unlike the mode I plot it is seen that $s \sim -\alpha^{1/2}$ for small α.

This case has the new feature that, since $y_e(\theta)$ has two peaks (recall the elastic result), two additional regions appear and the two angles θ_3 and θ_4 are required to describe the beginnings of the new reloading zone and the new unloading zone, respectively. The two angles θ_1 and θ_2 retain their old meanings. Table 4.1 shows values of s, θ_1, θ_2, θ_3, and θ_4 for $0.001 \le \alpha \le 1$. It is found, as depicted in Fig. 2.2c, that for $\alpha^+ < \alpha < 1$ ($0.3 < \alpha^+ < 0.5$) there is a four region solution: a plastic loading zone ahead of the crack, followed by a wide elastic unloading sector, followed by a thin plastic reloading sector, followed by another elastic unloading sector. For $\alpha^* < \alpha < \alpha^+$ ($0.05 < \alpha^* < 0.1$) there is a two region solution, and for $0 < \alpha < \alpha^*$ reloading occurs on the crack flank, and there is a three region solution. It should be noted that for $\alpha^+ < \alpha < 1$ two unloading conditions are needed, and the appropriate obvious notational changes were made in equations (3.19) and (3.20); for $0 < \alpha < \alpha^+$ the old formulation holds. By comparison to the mode III results we find that reloading on the crack flank occurs roughly at the same level of hardening (moderate), the singularity is a little stronger and the width of the reloading sector on the crack face is smaller. By comparison to the mode I results we find that for large strain-hardening the singularity is a little weaker, and reloading starts later and is less important. Finally, we observe that the trend of the values of θ_1 and θ_2 as $\alpha \to 0$ are

compatible with the corresponding mode II perfectly-plastic values (9.57° and 179.82°) of Slepyan (1974) for a material with a Tresca yield surface with $\nu = 1/2$.

Figure 4.2 shows plots of the particle effective stress as a function of θ for large, moderate, and small strain-hardening. It is noted that for large strain-hardening small changes from the elastic result take place, and the isolated plastic reloading zone is clearly observed. As α becomes smaller this initial reloading zone disappears, and for still lower values of α a thin plastic reloading zone appears on the crack flank. At the same time a flat variation in σ_e is approached ahead of the crack.

Figure 4.3 presents plots of the angular variations of the stresses $\bar{\sigma}_{r\theta}$, $\bar{\sigma}_{rr}$, $\bar{\sigma}_{\theta\theta}$, $\bar{\sigma}_{33}$, and $\bar{\sigma}_e$ for large, moderate, and small strain-hardening. For large α, the usual observations are made. For small α, we observe from this and Figure 4.4 (showing the angular variations of the Cartesian components of the stress) that the stress distribution agrees in character with the perfectly-plastic results of Slepyan (1974); we observe, for instance, a centered fan distribution developing ahead of the crack.

Figure 4.5 shows plots of the angular variations of the Cartesian components of the velocities $\bar{v}_1$ and $\bar{v}_2$. We remark that for small α they agree in form with the perfectly-plastic results of Slepyan (1974). They are of the same order of magnitude as the angular variations of the stresses, and they approach a constant level in the elastic unloading, and plastic reloading zones as $\alpha \to 0$.

5. Plane stress (mode I)

5.1 *Formulation.*

The variables for this geometry are the three non-zero components of the stress tensor $\sigma_{r\theta}$, σ_{rr}, $\sigma_{\theta\theta}$, and the two in-plane components of the velocity vector v_r, v_θ (v_3 does not enter the formulation of the problem). The governing equations are the two equilibrium

equations (3.1), (3.2), and the three in-plane components of the stress-strain relation (3.3) where we set σ_{33} equal to zero. These equations form a system of five first order PDE's in the five dependent variables identified above. If we now put

$$v_r(r,\theta) = V\,(\tau_o/E)\,y_1(\theta)\,r^s \qquad v_\theta(r,\theta) = V\,(\tau_o/E)\,y_2(\theta)\,r^s$$

$$\sigma_{r\theta}(r,\theta) = \tau_o\,y_3(\theta)\,r^s \qquad \sigma_{rr}(r,\theta) = \tau_o\,y_4(\theta)\,r^s \qquad \sigma_{\theta\theta}(r,\theta) = \tau_o\,y_5(\theta)\,r^s \tag{5.1}$$

into the five equations mentioned above, we obtain a system of five first order ODE's in the vector $\mathbf{y} = (y_1, y_2, \ldots, y_5)$

$$\mathbf{y}'(\theta) = \mathbf{f}(\theta, \mathbf{y}; s, \alpha, \nu) \tag{5.2}$$

where the components of $\mathbf{f}$ are given in Appendix A, and depend on whether loading or unloading occurs in the usual way.

Mode I symmetry ahead of the crack requires the three independent conditions

$$y_2(0) = y_3(0) = y_4'(0) = 0 \tag{5.3}$$

and vanishing tractions on the crack faces requires that

$$y_3(\pi) = y_5(\pi) = 0 \tag{5.4}$$

Thus we have five homogeneous boundary conditions to be satisfied by our fifth order system. As usual, s will be determined as the eigenvalue of the problem, and it will depend only on α. Similarly, we will be able to arbitrarily pick the amplitude factor of $\mathbf{y}(\theta)$.

Next we can use the usual arguments to show that the five dependent variables of the problem are continuous across any unloading or reloading boundary so that

$$[y_1] = [y_2] = \ldots = [y_5] = 0 \tag{5.5}$$

Similarly, we use the unloading condition (3.19) and the reloading condition (3.20) to determine θ_1 and θ_2 respectively.

Once again we use the same numerical scheme to perform the integration, but we need to get started by providing the values of $\mathbf{y}(0)$, $\mathbf{y}'(0)$, and s for a given α.

From (5.3) we have that $y_2(0) = y_3(0) = 0$. If we now pick $y_4(0) = 1$, and guess the values of $y_5(0)$ and s, we find using (5.2) that

$$y_1(0) = -s\,[y_4(0)/\alpha - \lambda\, y_5(0)] \tag{5.6}$$

and given that $y_4'(0) = 0$ we find that

$$\begin{aligned} y_1'(0) &= y_5'(0) = 0 \\ y_2'(0) &= -y_1(0) - s^2\,[y_5(0)/\alpha - \lambda\, y_4(0)] \\ y_3'(0) &= -(1+s)\, y_4(0) + y_5(0) \end{aligned} \tag{5.7}$$

We then integrate equations (5.1) numerically to find the values of $y(\theta)$ for $0 < \theta < \pi$. Given the values of $y_3(\pi)$ and $y_5(\pi)$, we check to see whether they vanish, and if they do not, we iterate in our guesses for $y_5(0)$ and s until convergence is achieved. The solutions are finally renormalised in the usual way ($y_e(\theta_1) = 1$) .

5.2 *Results*

In this case we produced results for a value of ν equal to 1/2, and several values of α. AH showed through their formulation of the problem that both s and the angular variations of the stresses are independent of ν. Only the angular variations of the velocities depend on ν. Figure 5.1 shows a plot of s versus $\alpha^{1/2}$, and we can see that $s \sim -\alpha^{1/2}$ for small α.

Table 5.1 shows values of s, θ_1, and θ_2 for $0.0001 \le \alpha \le 1$, and it also includes for comparison the values of s and θ_1 obtained by AH neglecting reloading. The loading history is depicted in Figure 2.2b. It is found that reloading occurs for all values of α such that $0 < \alpha < \alpha^*$ ($0.005 < \alpha^* < 0.01$), but that the width of the reloading sector is so small (less than 0.001°) that the values of s and θ_1 are virtually unaffected by reloading. As expected, for $\alpha^* < \alpha < 1$ our results agree very well with those of AH.

Figure 5.2 depicts plots of the particle effective stress for $0 < \theta < \pi$ for the three usual values of α. It is noted that for large strain-hardening a small perturbation from the elastic result occurs. As α becomes smaller the tiny reloading zone on the crack face appears, and the stress level ahead of the crack approaches a flat variation corresponding to the perfectly-plastic yield condition.

Figure 5.3 presents plots of the angular variations of the stresses for large, moderate, and small strain-hardening. The curves for large strain-hardening show little variation from the elastic result with the exception of $\bar{\sigma}_{rr}$ (and $\bar{\sigma}_e$) which becomes unbounded as $\theta \to \pi$. The results for small strain-hardening show that the stresses ahead of the crack are approaching a centered fan distribution. Figure 5.4 presents the corresponding angular variations of the Cartesian components of the stress tensor.

Figure 5.5 shows the angular variations of the Cartesian components of the velocity for the three values of α. We observe that they stay of the same order of magnitude as the stresses, and we can also see that they are nearly constant in the elastic unloading sector.

6. Plane stress (mode II)

6.1 *Formulation.*

The formulation of this problem is identical to that of the corresponding mode I problem with the exception of the boundary conditions ahead of the crack which for mode II become

$$y_1(0) = y_4(0) = y_5(0) = 0 \tag{6.1}$$

It is convenient here to pick the normalisation $y_3(0) = 1$, and we must guess the values of $y_2(0)$ and s for a given α. We can then use equations (5.2) to find

$$\begin{aligned} y_1'(0) &= (1-s)\, y_1(0) - 2s^2 [(1+\nu) + (3/2)(\alpha^{-1}-1)]\, y_3(0) \\ y_2'(0) &= y_3'(0) = 0 \\ y_5'(0) &= -(s+2)\, y_3(0) \end{aligned} \tag{6.2}$$

plus a more complicated expression for $y_4'(0)$. With these results we can start integrating equations (5.2) numerically, iterating in the values of $y_2(0)$ and s until a solution is found satisfying $y_3(\pi) = y_5(\pi) = 0$. Finally, we renormalise the solution in the usual way.

6.2 *Results.*

In this case we produced results for $\nu = 1/2$, and several values of α. Figure 6.1 is a plot of s versus $\alpha^{1/2}$, and it shows the usual behavior of $s \sim -\alpha^{1/2}$ for small α.

Table 6.1 shows values of s, θ_1, θ_2, θ_3, and θ_4 for $0.001 \leq \alpha \leq 1$. The four angles have the same interpretation as in the plane-strain mode II problem. The loading history is shown in Figure 2.2d. A four region solution is found for $\alpha^* < \alpha < 1$ ($0.1 < \alpha^* < 0.2$), a five region solution for $\alpha^+ < \alpha < \alpha^*$ ($0.01 < \alpha^+ < 0.05$), and a three region solution for $0 < \alpha < \alpha^+$. We remark that for $\alpha^* < \alpha < 1$ two unloading and one reloading conditions are needed, and for $\alpha^+ < \alpha < \alpha^*$ two unloading and two reloading conditions are needed. Thus for $\alpha^+ < \alpha < 1$ the appropriate obvious notation changes were made in equations (3.19) and (3.20), and for $0 < \alpha < \alpha^+$ the old formulation holds. Reloading starts at intermediate strain-hardening, and the size of the reloading zone is small but not as small as in mode I. The strength of the singularity is between that of the mode I (plane stress) and mode III problems. As $\alpha \to 0$ the values of θ_1 and θ_2 seem to be approaching limiting values that compare favorably with the perfectly-plastic values (13.31° and 179.61°) of Ponte (1985a).

Figure 6.2 depicts plots of the particle effective stress as a function of θ for large, moderate, and small strain-hardening. It is noted that for large strain-hardening small changes from the elastic result occur, and the isolated reloading zone is observed. As α becomes smaller the initial reloading zone disappears, and a new reloading zone appears on the crack flank. Simultaneously, the stress approaches a constant level in the plastic sector ahead of the crack.

Figure 6.3 presents plots of the angular variations of the stresses for the three usual values of α. Figure 6.4 presents a plot of the corresponding variations for the perfectly-plastic material. It is seen that the agreement between the small-α and perfectly-plastic results is very close.

Figure 6.5 shows plots of the angular variations of the Cartesian components of the velocity vector for the linear-hardening material. Figure 6.6 shows the corresponding variations for the perfectly-plastic material. Once again, remarkably, it appears that the linear-hardening variations approach the corresponding perfectly-plastic variations as α approaches zero.

7. Discussion of the small-α limit

It is natural to separate the perfectly-plastic problems into two groups according to their solutions. For the anti-symmetric modes (II and III), asymptotic solutions exist with continuous stress and velocity fields, and they have roughly the same configuration: a (singular) centered fan plastic sector ahead of the crack, followed by a (non-singular) elastic sector, followed, in turn, by a (non-singular) constant stress plastic sector on the crack flank. For the symmetric mode (I), fully-continuous solutions with the above, or other configurations have not been found, and presumably do not exist. For plane-strain mode I, a solution has been found (Rice *et al.*, 1980) which admits a discontinuity in the tangential component of the velocity vector at the plastic-plastic boundary ($\theta = 45°$) separating the constant stress sector ahead of the crack from the centered fan sector. For plane-stress mode I, no solution (of any type) seems yet to have been found.

On the other hand, our small-α numerical solutions to the linear-hardening problem seem to follow a similar pattern. For the anti-symmetric modes, the following features appear as $\alpha \to 0$: the strength of the singularity vanishes as $s \sim -c\,\alpha^{1/2}$ ($c > 0$), the angular variations of the stress and velocity fields seem to approach limits which agree with the corresponding perfectly-plastic variations, but the radial dependence of the velocities (r^s/s) does not approach the corresponding perfectly-plastic variation ($\ln r$), whereas that of the stresses does in a pointwise sense ($r^s \to 1$). For plane-strain mode I, s does not approach

zero, and neither do the angular variations of the velocities appear to approach a limit as α approaches zero, even though the angular variations of the stresses appear to approach a limit that is reminiscent of the Prandtl field. For plane-stress mode I, s does seem to approach zero as $\alpha \to 0$, and the angular variations of the fields also seem to approach a limit, but we were unsuccessful in relating this apparent limit to a perfectly-plastic solution with a similar configuration.

In this section we will first attempt to corroborate the observations from our numerical results that as $\alpha \to 0$, $s \sim -c\alpha^{1/2}$, and the angular variations of the fields of our small-α solutions approach the corresponding perfectly-plastic variations. We will second try to understand the breakdown as $\alpha \to 0$ of the radial dependence of our power singularity solution. For simplicity we will initially address these two questions in the context of the mode III problem, and then we will try to extend our conclusions to the mode II problems. Finally, we will have some comments about the mode I problems.

7.1 *Small-α eigenvalue and angular variations in mode III*

In Section 2 we solved numerically the eigenvalue problem given by the third order system (2.5) subject to consistency conditions that determined the value of $\underline{\alpha}$, and to the boundary conditions (2.9) and (2.10). It yielded as eigenvalue the strength of the singularity, and as eigenfunctions the angular variations of the power-singularity solution (2.4) to the linear-hardening problem. The problem was solved for several values of α ranging between zero and unity. The small-α results indicate that $s \sim -c\alpha^{1/2}$, and that the angular variations of the fields approach the corresponding perfectly-plastic variations. We would like to demonstrate that this is indeed the case. In order to accomplish this goal rigorously, we would need to produce an analytical expression for the small-α solution, and then take its limit as $\alpha \to 0$. However, we were not able to find such small-α solution, but we did find a solution to the eigenvalue problem corresponding to the value of $\alpha \equiv 0$. If

the small-α solution has a unique limit as $\alpha \to 0$, then it seems reasonable that this limit should agree with our $\alpha \equiv 0$ solution, which we derive below.

Equations (2.5) are in a form that is inconvenient to work with in the limit as $\alpha \to 0$, and they can be rewritten in the following fashion

$$y_2' + (1+s)\, y_1 = 0 \tag{7.1}$$

$$(s/\underline{\alpha})\, \sin\theta\, (y_1'-y_2)\, y_1 - (s^2/\underline{\alpha})\, (\cos\theta\, y_e^2 + \sin\theta\, y_1 y_2) - y_2 y_3' - s y_1 y_3 = 0 \tag{7.2}$$

$$y_1 y_3' - s\, [y_2 y_3 + \sin\theta\, (y_e^2 - y_2 y_1' + y_1 y_2')] = 0 \tag{7.3}$$

It is expected that as $\alpha \to 0$, $s \to 0$ so that for $\alpha \equiv 0$, we take $s \equiv 0$. Then (7.1) takes the simplified form

$$y_2' + y_1 = 0 \tag{7.4}$$

In the elastic sector $\underline{\alpha} = 1$, and (7.2) and (7.3) reduce to

$$\sin\theta\, (y_1'-y_2) - y_3 = 0 \tag{7.5}$$

$$y_3' = 0 \tag{7.6}$$

for otherwise we would have to require that $y_1 = y_2 = 0$. The solution of (7.4) to (7.6) is

$$\begin{aligned} y_1 &= A \sin\theta + C \cos\theta + B\, (\theta \sin\theta + \cos\theta \ln|\sin\theta|\,) \\ y_2 &= A \cos\theta - C \sin\theta + B\, (\theta \cos\theta - \sin\theta \ln|\sin\theta|\,) \\ y_3 &= B \end{aligned} \tag{7.7}$$

In the plastic sectors $\underline{\alpha} = \alpha$. In order to have an appropriate balance of terms in (7.2), we need to let either s/α or s^2/α approach a constant non-zero value as $\alpha \to 0$. Our numerical results support the second possibility: $s^2/\alpha \to k$. Then (7.3) allows us to identify two cases:

(i) $y_1 = 0$ (7.8a)

In this case (7.4) yields

$$y_2 = 1 \tag{7.8b}$$

where we have picked a normalisation, and it follows from (7.2) and (7.3) that

$$y_3 = -\sin\theta \tag{7.8c}$$

and $k = 1$.

(ii) $y_3' = 0$

Then (7.2) yields

$$y_1' - y_2 = 0$$

which together with (7.4) yields

$$y_1 = a \sin\theta + c \cos\theta \tag{7.9a}$$

$$y_2 = a \cos\theta - c \sin\theta \tag{7.9b}$$

Also

$$y_3 = b \tag{7.9c}$$

In order to construct a solution to the full problem we assume that equations (7.8), which obey the boundary conditions at $\theta = 0$, hold in the interval $0 < \theta < \theta_1$, equations (7.7) hold in $\theta_1 < \theta < \theta_2$, and equations (7.9) with $a = 0$ (in order to satisfy the boundary condition at $\theta = \pi$) hold in $\theta_2 < \theta < \pi$. We then impose continuity of the stresses and velocity at the two boundaries, the unloading condition which in this case is superfluous, and the reloading condition which yields $|c| = 1$. The result, not very surprisingly, agrees with the angular variations of the perfectly-plastic fields (see Appendix B), and demonstrates (under the presumption that the small-α solution has a unique limit) the validity of the original assertion.

7.2 *Small-α radial dependence in mode III*

The radial dependence of the velocity in our power-singularity solution to the linear-hardening problem suffers from the difficulty that it becomes unbounded as α (and hence s) approaches zero. We observe however that for $e^{-1/|s|} << r << 1$

$$r^s = e^{s \ln r} = 1 + s \ln r + \ldots \tag{7.10}$$

so that

$$r^s/s = 1/s + \ln r + \ldots \tag{7.11}$$

This suggests that adding solutions with eigenvalues of opposite signs would yield the correct (perfectly-plastic) radial dependence for both the velocity and the stresses in the

limit as $\alpha \to 0$, provided that the angular variations corresponding to both eigenvalues approached the same limit. Moreover, it is apparent from the discussion in the previous section that if a solution with the specified balance of terms in the limit ($s^2/\alpha \to$ constant) exists, the limiting angular variations are insensitive to the sign of the eigenvalue. However, because the linear-hardening equations are nonlinear, we cannot expect in general that the sum of two such solutions with eigenvalues of opposite sign will also be a solution, but in this problem it happens that in the limit as $\alpha \to 0$ the equations in the plastic sectors become linear (in the elastic sector they are always linear) so that the sum yields in the limit a solution to the linear-hardening problem which is precisely the perfectly-plastic solution. In order to give some plausibility to the above ideas we will study the following *model* problem.

Consider the eigenvalue problem specified by equations (2.2) and (2.3) with $\underline{\alpha} = \alpha$, subject to the homogeneous boundary conditions

$$\tau_r(r,0) = v_3(r,0) = 0$$
$$\tau_e^{\cdot}(r,\theta_1) = 0 \tag{7.12}$$

where $\theta_1 = \pi/2$. Two solutions to this problem are

$$\boldsymbol{\tau}^* = \tau_o\, r^{s^*}\, \mathbf{e}_\theta \qquad v_3^* = -V\,(\tau_o/G)\sin\theta\, r^{s^*}/\, s^* \tag{7.13}$$

with $s^* = \pm\alpha^{1/2}$ as eigenvalues. Note that

$$\tau_e^{\cdot *} = -s^*\,\tau_o\,(V/R)\cos\theta\, r^{s^*-1} \tag{7.14}$$

It follows that $\tau_e^{\cdot *}(r,\theta_1) = 0$, and that for $0 < \theta < \theta_1$, $\tau_e^{\cdot *}(r,\theta) > 0$ (< 0) for $s^* = -\alpha^{1/2}$ ($+\alpha^{1/2}$) so that of the two possible eigenvalues only the negative one is physically acceptable, since we have assumed plastic loading.

Further note that the velocity in each solution becomes unbounded as $\alpha \to 0$. However, surprisingly, the addition of the two solutions yields an exact solution to the (nonlinear) governing equations, and boundary conditions. Thus

$$\tau^* = \tau_o [(r^{\sqrt{\alpha}} + r^{-\sqrt{\alpha}})/2] \, e_\theta = \tau_o \cosh(\alpha^{1/2} \ln r) \, e_\theta$$

$$v_3^* = -V (\tau_o/G) \sin\theta \, (r^{\sqrt{\alpha}} - r^{-\sqrt{\alpha}}) / (2\alpha^{1/2}) = -V (\tau_o/G) \sin\theta \sinh(\alpha^{1/2} \ln r) / \alpha^{1/2} \tag{7.15}$$

is another solution to our model problem. This solution was first obtained through a different procedure by Dunayevsky and Achenbach (1982). Note that

$$\tau_e'^* = -\alpha^{1/2} \tau_o (V/R) \cos\theta \sinh(\alpha^{1/2} \ln r) / r \tag{7.16}$$

satisfies $\tau_e'^*(r,\theta_1) = 0$, and $\tau_e'^*(r,\theta) > 0$ for $0 < \theta < \theta_1$ so that (7.15) is also a physical solution. In addition, this solution has the desirable property that it is well-defined in the limit as $\alpha \to 0$

$$\tau^* = \lim_{\alpha \to 0} \{ \tau_o \cosh(\alpha^{1/2} \ln r) \, e_\theta \} = \tau_o e_\theta$$

$$v_3^* = -\lim_{\alpha \to 0} \{ V (\tau_o/G) \sin\theta \sinh(\alpha^{1/2} \ln r) / \alpha^{1/2} \} = -V (\tau_o/G) \sin\theta \ln r \tag{7.17}$$

We remark that these are the fields (corresponding to a centered fan sector) which would be the solution of the corresponding perfectly-plastic model problem; this demonstrates that the governing equations of a linear-hardening problem, at least for some configurations, admit solutions that approach the corresponding perfectly-plastic solutions in the limit as $\alpha \to 0$.

In our model problem we find that the power singularity solution to the linear-hardening equations is not general enough to yield the full perfectly-plastic solution in the limit, but does yield the correct angular variations of the eigenfunctions. By adding an appropriate nonsingular (mathematical) solution to the power-singularity solution we are able to obtain the full perfectly-plastic solution in the limit.

We are now in the position to make an estimate for the range of validity of the power singularity in the model problem. We pointed out in (7.10) that for $e^{-1/|s|} << r << 1$, $r^s \sim 1$. Therefore, only when $0 < r << e^{-1/\sqrt{\alpha}}$ are we justified in neglecting $r^{\sqrt{\alpha}}$ compared to $r^{-\sqrt{\alpha}}$. Hence, the range of validity of the power singularity solution (7.13) to the model

problem is given by $0 < r << e^{-1/\sqrt{\alpha}}$, and we remark that this domain vanishes as $\alpha \to 0$, as observed by Dunayevsky and Achenbach (1982).

The properties of the model problem are very suggestive, and we would expect that at least some of these features would apply to the full problem. Indeed, it appears that the full problem may have another (mathematical) solution with a positive eigenvalue that would have the same limit for the angular variations of the fields and the radial dependence of the stresses as the power singularity solution (and the perfectly-plastic solution). However, the radial dependence of its velocity would have a singular term in α that in the limit has the opposite sign of the corresponding singular term in the radial dependence of the velocity of the power singularity solution. Then the sum of these two solutions, which is not a solution to the linear-hardening equations for general α, would in the limit as $\alpha \to 0$ become a solution to the full linear-hardening problem, and agree with the solution to the perfectly-plastic problem. It is conceivable that one might be able to construct a uniformly valid solution to the small-α problem (analogous to (7.15) in the model problem) that would rigorously demonstrate the above ideas, but such a solution, if it exists, has yet to be found. On the other hand, one might expect that the behavior of such small-α solution might not be very different in character from (7.15), and thus expect a similar range of validity for our power singularity solutions to the full linear-hardening problem.

7.3 *The mode II problems*

As we have already pointed out, similar observations from our numerical small-α solutions were made for plane-stress and plane-strain mode II. It seems plausible that the same ideas developed for the mode III problem may apply here, but the technical difficulties involved are even greater. Based on these comments we expect the range of validity of our power singularity solutions to be roughly the same as that for mode III.

7.4 *The mode I problems*

For plane-strain mode I, we have already observed that the eigenvalue of the power-singularity solution does not approach zero as $\alpha \rightarrow 0$, and also that the angular variations of the velocities do not appear to approach a limit. Alternatively, the perfectly-plastic solution involves discontinuities in the velocity, so that it might be conjectured that due to the fact that our numerical formulation implicitly assumes continuity of the velocity, our formulation of the linear-hardening problem may become overdetermined as $\alpha \rightarrow 0$, and thus yield a spurious limit for s.

For plane-stress mode I, the small-α solutions seem to indicate that a limit is approached with fully continuous fields. But when we searched for a perfectly-plastic solution with that configuration we failed. This may be an indication that the small-α results may not actually be approaching a valid limit, in accordance with the plane strain case.

Hence for the symmetric mode problems we expect our power singularity solutions to be of limited relevance for small α, and their ranges of validity to be even smaller than those of the anti-symmetric modes.

8. Concluding Remarks

It was found that reloading on the crack flanks of the growing crack in the linear-hardening material occurs for all values of α less than a critical value α^* where $\alpha^* < 1$. On the other hand, it was also found that the angular variation (fixed r) of the effective stress $\bar{\sigma}_e$ becomes unbounded on the crack faces for any amount of plasticity in a linear-hardening material ($0 < \alpha < 1$). These two observations seem to be in contradiction. To see that they are really not, we recall that the definition of reloading involves a fixed particle ($x_2 = \bar{x}_2$). Hence, even though the angular variation of the effective stress of a particle

becomes unbounded as the particle travels far into the wake of the crack ($\bar{\theta} \to \pi$), the radial variation (r^s) of the same stress vanishes, and the product of the two, namely, the effective stress of the particle approaches a finite level, $\sigma_e{}^w$. We expect $\sigma_e{}^w$ to be a continuous function of α, and we know that it vanishes for the elastic problem ($\alpha = 1$). On the other hand reloading does not occur until $\sigma_e{}^w$ exceeds the effective stress, $\sigma_e{}^1$, that the particle had at unloading. Hence, it follows that $\alpha^* < 1$.

It was found that the size of the plastic reloading sector is small (less than 0.5°) for all cases except for plane-strain mode I where the width of the reloading sector exceeded 40° for small α. We also note that the width of the reloading sector for the plane-stress mode I problem is significantly smaller (less that 0.001°) than for all the other cases. Thus it turns out that, with the exception of the plane-strain mode I problem, the effect of reloading on the global properties of the solution (the strength of the singularity, s, and the size of the primary plastic loading sector, θ_1) is small, so that the approximation of AH is a good one. On the other hand, in the plane-strain mode I problem we found that the effect of reloading on s and θ_1 is sizeable; however, although the effect is consistent in the sense that it makes s weaker for small α, it does not change the character of the solution significantly. In any case the intuitive expectation that reloading should become relatively more important as the perfectly-plastic limit is approached was verified for all cases.

The mode II results agree in general terms with those of the simpler mode III case. They show a similar functional dependence of s, θ_1, and θ_2 on α, and a similar small-α behavior. On the other hand, the mode II results introduce the new feature that for large α a small reloading sector floating in the middle of the elastic unloading sector is observed, which allows for interesting particle loading histories, but this feature disappears for smaller α.

Some progress was made in understanding the small-α limit of the power singularity solutions to the linear-hardening problem. For the anti-symmetric modes (II and III), we are inclined to think that the small-α solutions approach limits which are related to

the perfectly-plastic solutions. In fact, the angular variations of the small-α limits approach those of the perfectly-plastic solutions. However, due to the singular nature (in α) of the radial dependence of the velocity in these solutions, their range of validity $(0 < r << e^{-1/\sqrt{\alpha}})$ vanishes as $\alpha \rightarrow 0$. On the other hand, for the symmetric mode problems, it appears that our small-α solutions are completely unrelated to the perfectly-plastic solutions.

Even though the validity of our small-α results may be restricted, the results for moderate and large strain-hardening should prove to be applicable to appropriate materials (such as reinforced ceramics), where these near-tip solutions may be embedded in finite-element calculations of the full fields of a steadily propagating crack.

Aknowledgements

This work was supported in part by the Office of Naval Research under Contract N00014-84-K-0510, and by the Division of Applied Sciences, Harvard University. The author is grateful to B. Budiansky for suggesting this project and for his valuable comments, and to J. W. Hutchinson and P. A. Mataga for helpful discussions.

References

Amazigo, J.C. and Hutchinson, J.W., "Crack-tip fields in steady crack growth with linear strain-hardening", *J. Mech. Phys. Solids*, **25**, 81-97 (1977).

Chitaley, A.D. and McClintock, F.A., "Elastic-plastic mechanics of steady crack growth under anti-plane shear", *J. Mech. Phys. Solids*, **19**, 147-163 (1971).

Drugan, W.J., Rice J.R. and Sham, T.L., "Asymptotic analysis of growing plane strain tensile cracks in elastic-ideally plastic solids", *J. Mech. Phys. Solids*, **30**, 447-473 (1982).

Dunayevsky, V. and Achenbach, J.D., "Radial nonuniformity of the fields near a moving crack tip in a material with linear strain-hardening", *J. Appl. Mech.*, **49**, 646-647 (1982).

Gao, Y.-C., "Elastic-plastic field at the tip of a crack growing steadily in perfectly-plastic medium" (in Chinese), *Acta Mechanica Sinica*, **1**, 48-56 (1980).

Gao, Y., Zhang, X. and Hwang, K., "The asymptotic near-tip solution for mode III crack in steady growth in power hardening media", *Int. J. of Fract.*, **21**, 301-317 (1983).

Lo, K. K. and Pierce, D., "Effect of a yield surface vertex on crack-tip fields in Mode III", *J. Mech. Phys. Solids*, **29**, No. 2, 143-152 (1981).

Ponte Castañeda, P., "Asymptotic fields of a perfectly-plastic, plane-stress mode II growing crack", Harvard University, Division of Applied Sciences, Report MECH-70 (1985a)

Ponte Castañeda, P., "Asymptotic analysis of a mode I crack propagating steadily in a deformation theory material", Harvard University, Division of Applied Sciences, Report MECH-71 (1985b)

Rice, J.R., Drugan, W.J. and Sham, T.L., "Elastic-plastic analysis of growing cracks", *Fracture Mechanics: Twelfth Conference*, ASTM-STP 700, 189-219 (1980).

Rice, J.R., "Elastic-plastic crack growth", *Mechanics of Solids: The Rodney Hill 60th Anniversary Volume* (ed. by H.G. Hopkins and M.J. Sewell), Pergamon Press, Oxford, 539-562 (1982)

Slepyan, L.I., "Deformation at the edge of a growing crack", *Mekhanika Tverdogo Tela*, **8**, 139-148 (1973).

Slepyan, L.I., "Growing crack during plane deformation of an elastic-plastic body", *Mekhanika Tverdogo Tela*, **9**, 57-67 (1974).

Zhang, R., Zhang, X. and Hwang, K., "Near-tip fields for plane strain mode I steady crack growth in linear-hardening material with Bauschinger effect", *Proceedings of ICF International Symposium on Fracture Mechanics* (ed. by K. Hwang, C. Liu, and Q. He), Science Press, Beijing (1983).

Appendix A. *The governing systems of O.D.E's.*

Anti-plane strain

$$f_1 = (\sin\theta\, T_1)^{-1} [\ (s/\underline{\alpha}) \cos\theta\, y_1 + \sin\theta\, T_2\, y_2 + y_3\ ]$$

$$f_2 = -(s + 1)\, y_1$$

$$f_3 = -s^2 \sin\theta\, y_1 - s^2 \cos\theta\, y_2 - s\,(\underline{\alpha}^{-1} - 1)\, T_3\, y_2 + s\,(\underline{\alpha}^{-1} - 1) \sin\theta\ \bar{y}_1\, \bar{y}_2\, f_1$$

where

$$T_1 = [\ 1 + (\underline{\alpha}^{-1} - 1)\, \bar{y}_1^2\ ]$$

$$T_2 = [\ 1 + (\underline{\alpha}^{-1} - 1)\, (s+1)\, \bar{y}_1^2\ ]$$

$$T_3 = [\ s \cos\theta + (s+1) \sin\theta\, \bar{y}_1\, \bar{y}_2\ ]$$

and

$$\bar{y}_i = (y_i / y_e)$$

Plane strain.

$$f_1 = (1-s)\, y_2 - 2s^2 \cos\theta\, [\ (1+\nu) + (3/2)\, (\underline{\alpha}^{-1} - 1)\ ]\, y_3 - 2s \sin\theta\, T_1$$

$$f_2 = -y_1 - s^2 \cos\theta\, [\ z_5 + (\underline{\alpha}^{-1} - 1)\, x_5\ ] - s \sin\theta\, T_2$$

$$f_3 = -(1+s)\, y_4 + y_5$$

$$f_4 = (1/\sin\theta)\, T_3\, \{\ \ldots\ \}$$

$$f_5 = -(s+2)\, y_3$$

$$f_6 = (1/\sin\theta)\, T_3\, \{\ \ldots\ \}$$

where

$$T_1 = s\,(1+\nu)\, y_4 - (3/2)\, (\underline{\alpha}^{-1} - 1)\, \bar{y}_3\, f_e$$

$$T_2 = s\, y_3 + \nu\, (f_4 - 2y_3 + f_6) - (\underline{\alpha}^{-1} - 1)\, \bar{x}_5\, f_e$$

$$T_3 = \{[1 + (\underline{\alpha}^{-1} - 1)\, \bar{x}_4^2][1 + (\underline{\alpha}^{-1} - 1)\, \bar{x}_6^2] - [\nu - (\underline{\alpha}^{-1} - 1)\, \bar{x}_4\, \bar{x}_6]^2\}^{-1}$$

$$f_e = y_e'$$

$$x_4 = y_4 - (1/2)\, (y_5 + y_6) \qquad x_5 = y_5 - (1/2)\, (y_4 + y_6) \qquad x_6 = y_6 - (1/2)\, (y_4 + y_5)$$

$$z_4 = y_4 - \nu\, (y_5 + y_6) \qquad z_5 = y_5 - \nu\, (y_4 + y_6) \qquad z_6 = y_6 - \nu\, (y_4 + y_5)$$

Plane stress.

$$f_1 = (1-s)\, y_2 - 2s^2 \cos\theta \left[(1+\nu) + (3/2)\, (\underline{\alpha}^{-1} - 1) \right] y_3 - 2s \sin\theta\, T_1$$

$$f_2 = -y_1 - s^2 \cos\theta \left[z_5 + (\underline{\alpha}^{-1} - 1)\, x_5 \right] - s \sin\theta\, T_2$$

$$f_3 = -(1+s)\, y_4 + y_5$$

$$f_4 = (1/\sin\theta) \left[1 + (\underline{\alpha}^{-1} - 1)\, \bar{x}_4^2 \right]^{-1} \left\{ y_1 + s \cos\theta\, T_3 + \sin\theta\, T_4 \right\}$$

$$f_5 = -(s+2)\, y_3$$

where

$$T_1 = s\,(1+\nu)\, y_4 - (3/2)\, (\underline{\alpha}^{-1} - 1)\, \bar{y}_3\, f_e$$

$$T_2 = s\, y_3 + \nu\, (f_4 - 2y_3) - (\underline{\alpha}^{-1} - 1)\, \bar{x}_5\, f_e$$

$$T_3 = \left[z_4 + (\underline{\alpha}^{-1} - 1)\, x_4 \right]$$

$$T_4 = \left[(2-s\nu)\, y_3 - (\underline{\alpha}^{-1} - 1)\, (3 y_3 f_3 + x_5 f_5)\, \bar{x}_4^2 \right]$$

$$f_e = y_e'$$

$$x_4 = y_4 - (1/2)\, y_5 \qquad x_5 = y_5 - (1/2)\, y_4$$

$$z_4 = y_4 - \nu\, y_5 \qquad z_5 = y_5 - \nu\, y_4$$

Appendix B. *The perfectly-plastic solution for anti-plane strain*

Centered fan plastic sector $(0 < \theta < \theta_1)$

$$\boldsymbol{\tau} = \tau_o \, \mathbf{e}_\theta$$

$$v_3 = -V \, (\tau_o/G) \sin\theta \ln r$$

Elastic unloading sector $(\theta_1 < \theta < \theta_2)$

$$\boldsymbol{\tau} = \tau_o \, [\, (C + B \ln|\sin\theta| \,) \, \mathbf{e}_1 + (A + B \, \theta \,) \, \mathbf{e}_2 \,]$$

$$v_3 = V \, (\tau_o/G) \, B \ln r$$

Constant stress sector $(\theta_2 < \theta < \pi)$

$$\boldsymbol{\tau} = \tau_o \, \mathbf{e}_1$$

$$v_3 = V \, (\tau_o/G) \, B \ln r$$

where

$$A = \cos\theta_1 + \theta_1 \sin\theta_1$$

$$B = -\sin\theta_1$$

$$C = \sin\theta_1 \, [\, \ln|\sin\theta_1| - 1]$$

$$\theta_1 \approx 19.7112^\circ$$

$$\theta_2 \approx 179.6334^\circ$$

Tables

Table 2.1.- Mode III

α	s	s^*	θ_1	$\theta_1{}^*$	θ_2
1.	-0.5	-0.5	90.00	90.0	
0.75	-0.455		87.79		
0.67	-0.437		86.83		
0.5	-0.394	-0.394	84.39	84.4	
0.3	-0.325	-0.325	79.81	79.8	
0.2	-0.277	-0.277	76.09	76.2	
0.1	-0.207	-0.207	69.82	70.0	
0.05	-0.153		63.98		179.999
0.01	-0.0733	-0.0737	52.88	52.0	179.947
0.005	-0.0528		49.21		179.912
0.001	-0.0244	-0.0244	42.88	43.0	179.840
0.000001	-0.00081		33.88		179.731

(*) Results from Amazigo and Hutchinson neglecting reloading.

Table 3.1.- Plane strain mode I $\nu = 1/3$

α	s	s^*	θ_1	θ_1^*	θ_2
1.	-0.5	-0.5	88.62	88.6	
0.75	-0.478		91.91		
0.67	-0.469		93.65		
0.5	-0.442	-0.442	98.40	98.4	
0.3	-0.373	-0.373	107.46	107.4	
0.2	-0.300		113.88		179.68
0.1	-0.197	-0.197	123.35	124.6	173.61
0.05	-0.142	-0.136	130.61	137.1	160.95
0.01	-0.0797	-0.0887	135.19	156.8	145.47
0.005	-0.0676		136.07		141.87
0.001	-0.0560		137.00		138.36

(*) Results from Amazigo and Hutchinson neglecting reloading.

Table 4.1.- Plane strain mode I $\nu = 1/3$

α	s	θ_1	θ_3	θ_4	θ_2
1.	-0.5	42.22	128.76	137.66	
0.75	-0.464	41.44	129.45	136.94	
0.67	-0.449	41.10	129.99	136.63	
0.5	-0.413	40.22	132.79	135.85	
0.3	-0.349	38.43			
0.2	-0.301	36.89			
0.1	-0.229	34.12			
0.05	-0.170	31.39			180.00
0.01	-0.0822	25.90			179.97
0.005	-0.0594	24.03			179.95
0.001	-0.0275	20.76			179.91

Table 5.1.- Plane stress mode I $\nu = 1/2$

α	s	s^*	θ_1	$\theta_1{}^*$	θ_2
1.	-0.5	-0.5	79.92	79.9	
0.75	-0.468	-0.468	80.78	80.8	
0.67	-0.455		80.90		
0.5	-0.420		80.76		
0.3	-0.357		79.34		
0.2	-0.310		78.58		
0.1	-0.237	-0.237	73.65	73.6	
0.05	-0.178	-0.178	69.53	69.6	
0.01	-0.0863	-0.0864	61.09	61.1	180.000
0.005	-0.0623	-0.0624	58.23	58.3	179.999
0.001	-0.0287		53.20		179.999
0.0001	-0.00925		49.00		180.000

(*) Results from Amazigo and Hutchinson neglecting reloading.

Table 6.1.- Plane stress mode II $\nu = 1/2$

α	s	θ_1	θ_3	θ_4	θ_2
1.	-0.5	46.35	102.58	134.13	
0.75	-0.456	45.81	101.61	132.83	
0.67	-0.439	45.57	101.33	132.28	
0.5	-0.398	44.93	100.96	130.91	
0.3	-0.332	43.62	101.37	128.46	
0.2	-0.286	42.44	102.62	126.57	
0.1	-0.219	40.27	106.56	123.50	180.00
0.05	-0.166	38.01	114.84	120.34	179.99
0.01	-0.0795	31.91			179.91
0.005	-0.0572	29.79			179.87
0.001	-0.0263	26.13			179.79

Figures

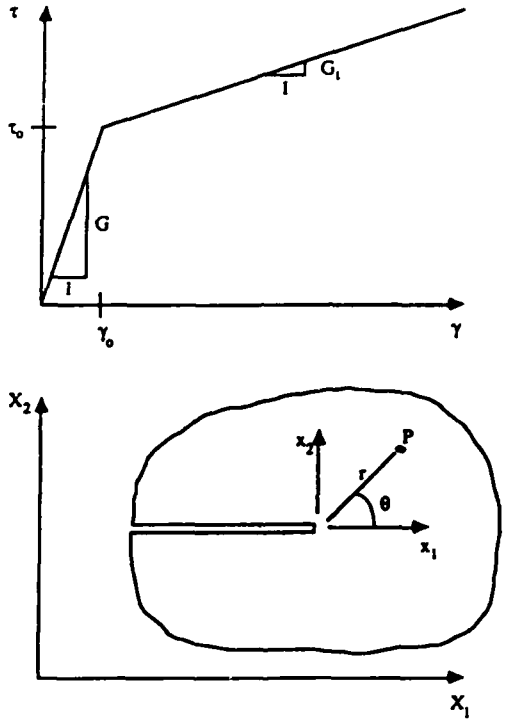

Figure 2.1— Crack-tip geometry and stress-strain curve.

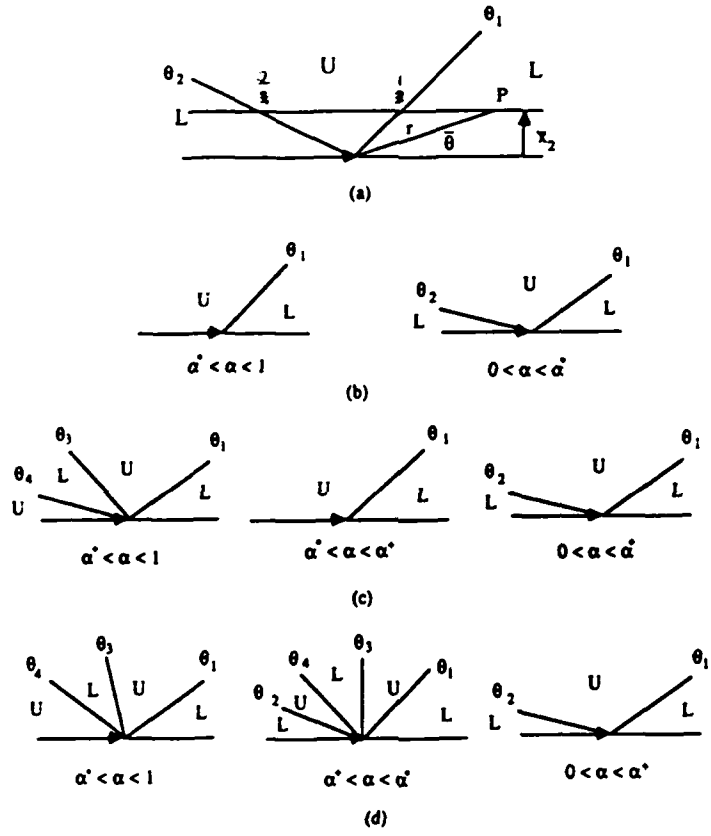

Figure 2.2—(a) Loading history of particle P: it loads plastically (L) ahead of the crack, unloads elastically (U) at 1, and reloads plastically (L) at 2. Loading history as a function of α for modes III and I (b), plane-strain mode II (c), and plane-stress mode II (d).

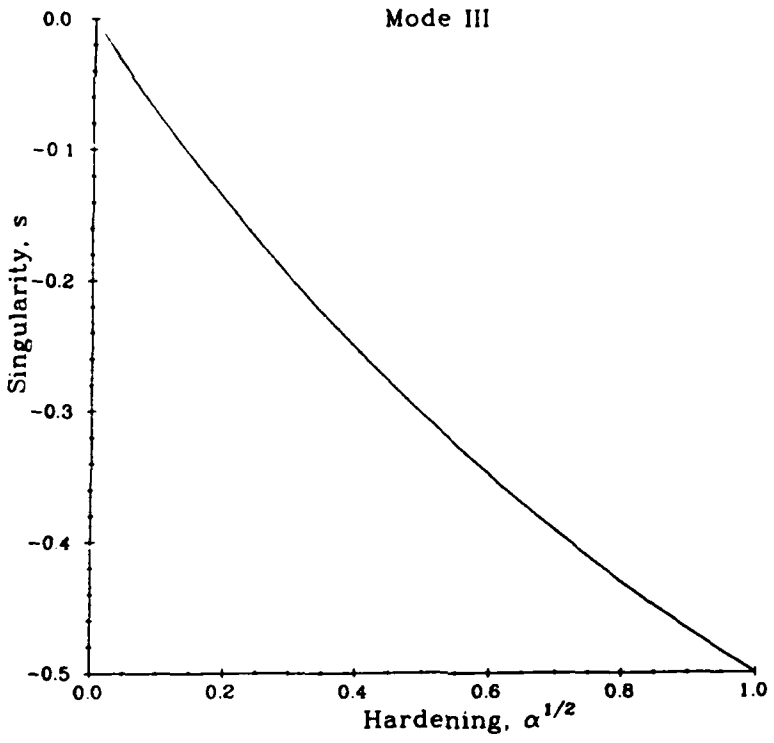

Figure 2.3—Strength of the singularity in anti-plane shear.

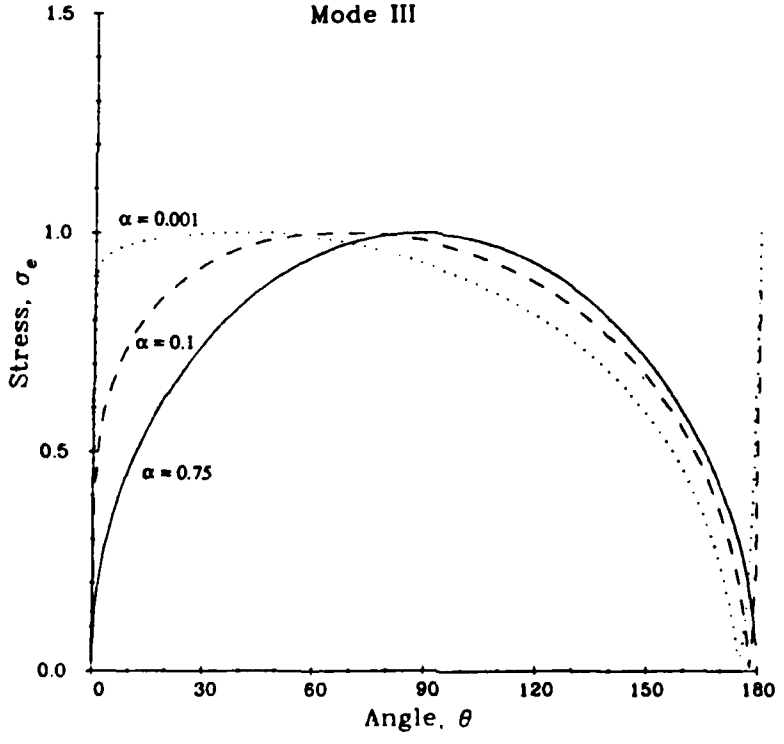

Figure 2.4—Particle (x_2 fixed) effective stress distribution in anti-plane shear for large, moderate, and small strain-hardening, normalised such that $\tau_e(r,\theta_1) = 1$.

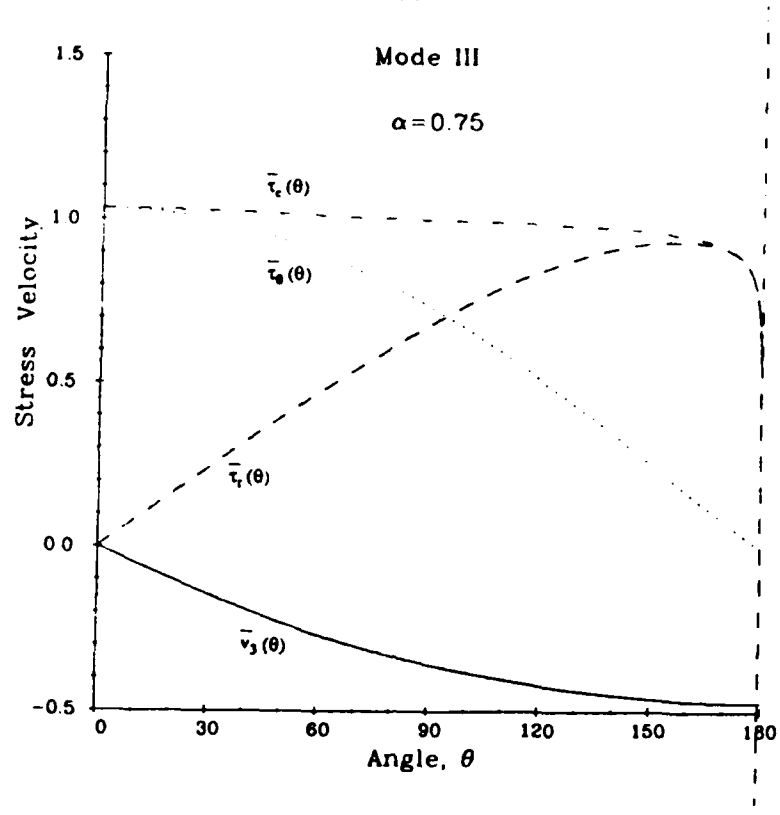

Figure 2.5a—Angular (r fixed) stress and velocity distribution in anti-plane shear for large strain-hardening, normalised such that $\bar{\tau}_e(\theta_1) = 1$.

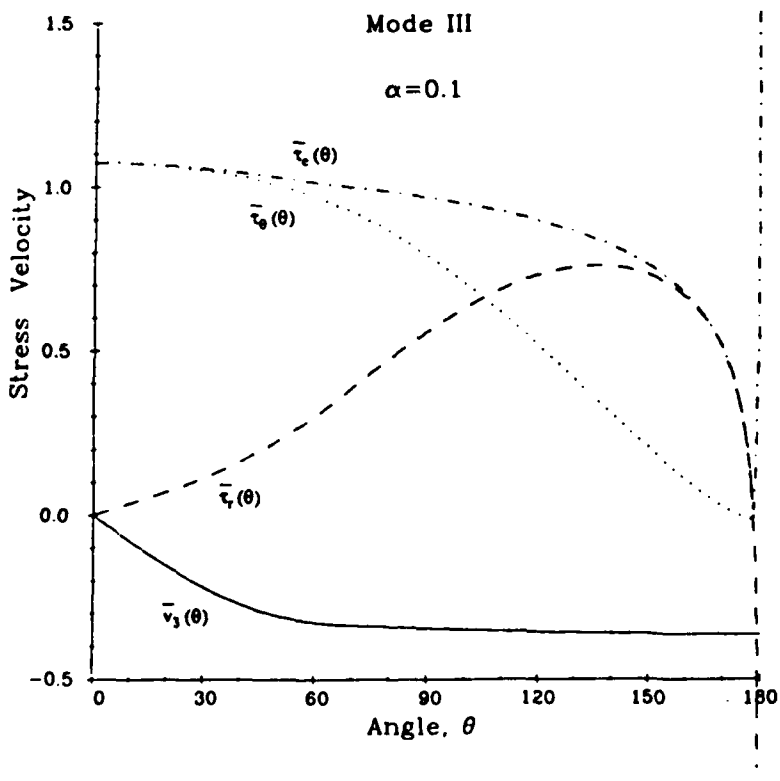

Figure 2.5b—Angular stress and velocity distribution in anti-plane shear for moderate strain-hardening, normalised such that $\bar{\tau}_e(\theta_1) = 1$.

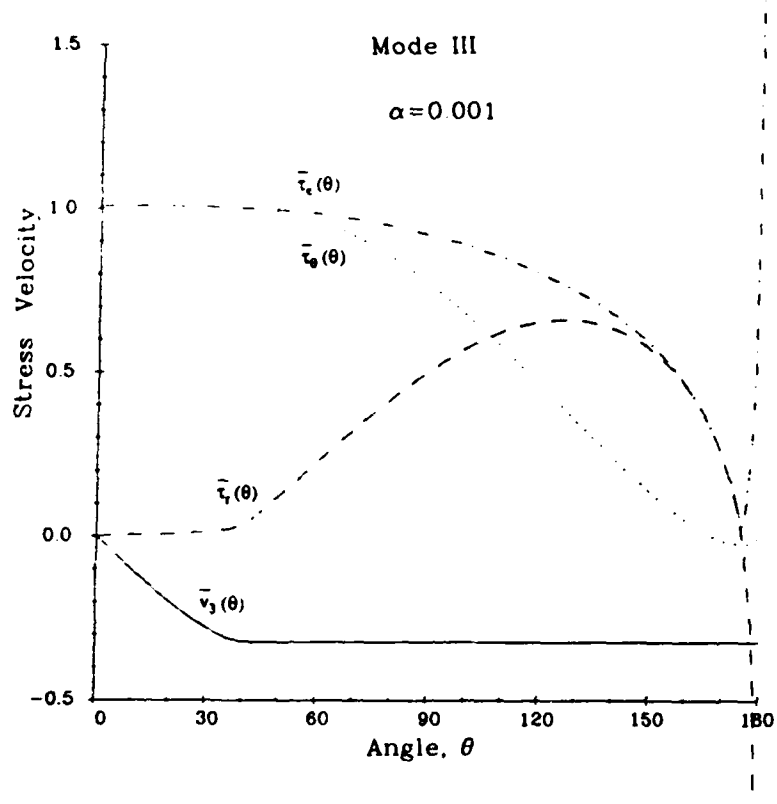

Figure 2.5c—Angular stress and velocity distribution in anti-plane shear for small strain-hardening, normalised such that $\bar{\tau}_e(\theta_1) = 1$.

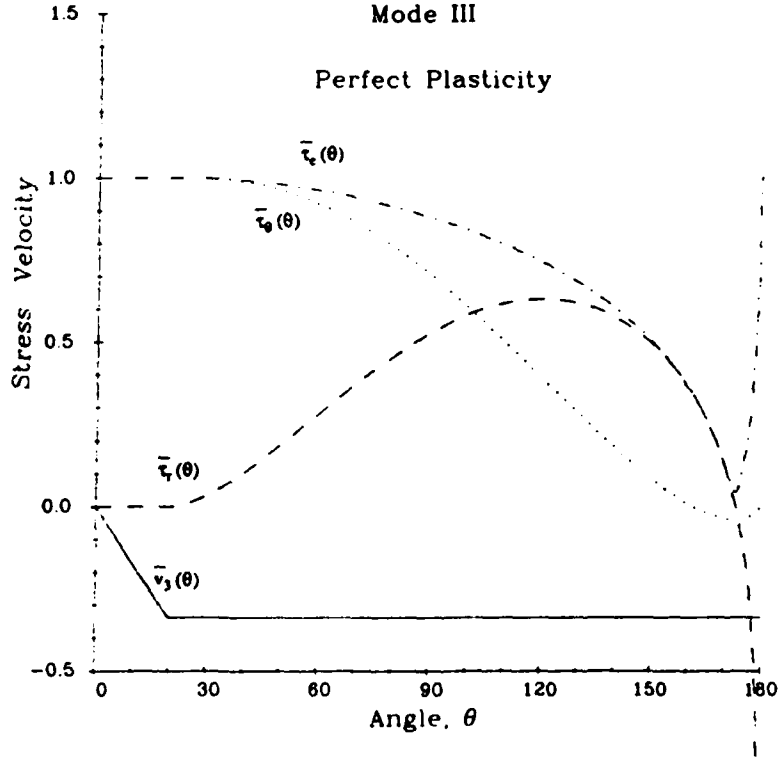

Figure 2.6— Angular stress and velocity distribution in anti-plane shear for perfect-plasticity, normalised such that $\tau_o = 1$.

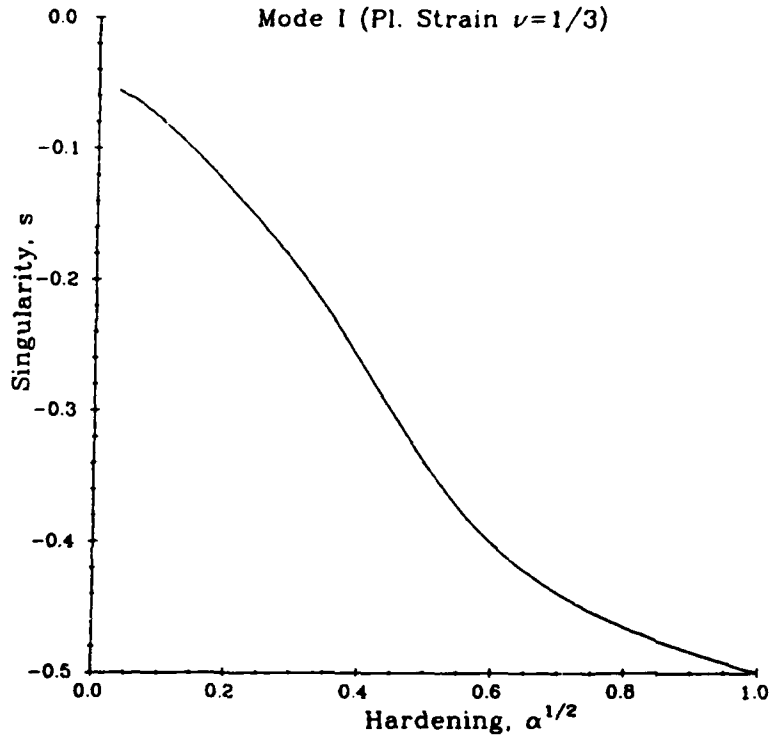

Figure 3.1—Strength of the singularity in plane strain mode I ($\nu = 1/3$).

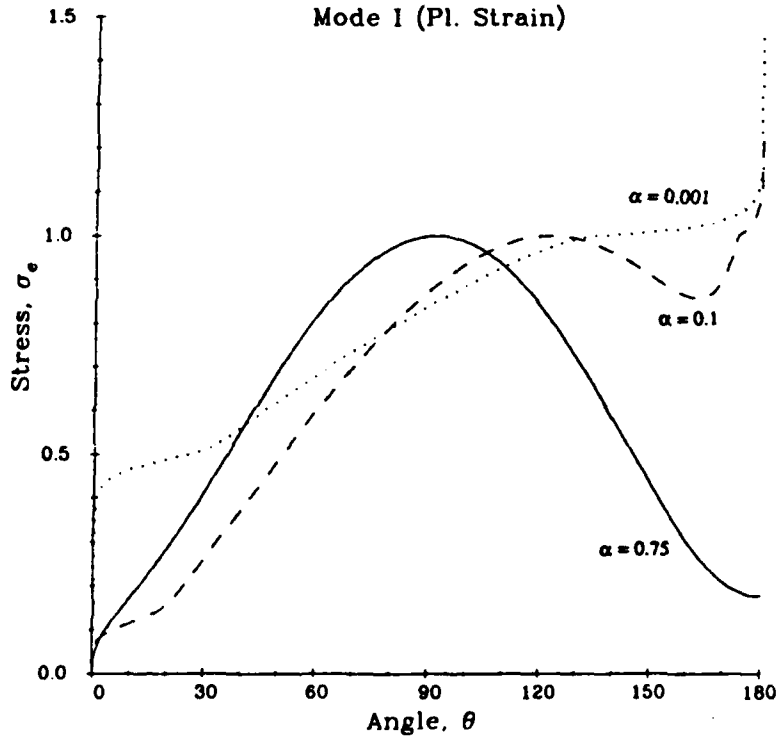

Figure 3.2—Particle effective stress distribution in plane strain mode I for large, moderate, and small strain-hardening, normalised such that $\sigma_e(r,\theta_1) = 1$.

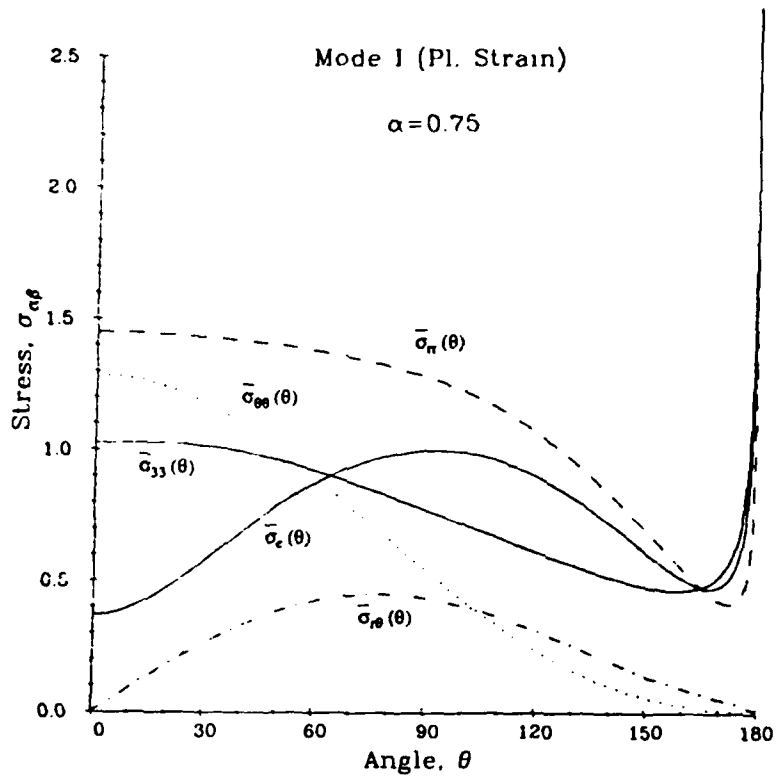

Figure 3.3a—Angular stress distribution in plane strain mode I for large strain-hardening, normalised such that $\bar{\sigma}_e(\theta_1) = 1$.

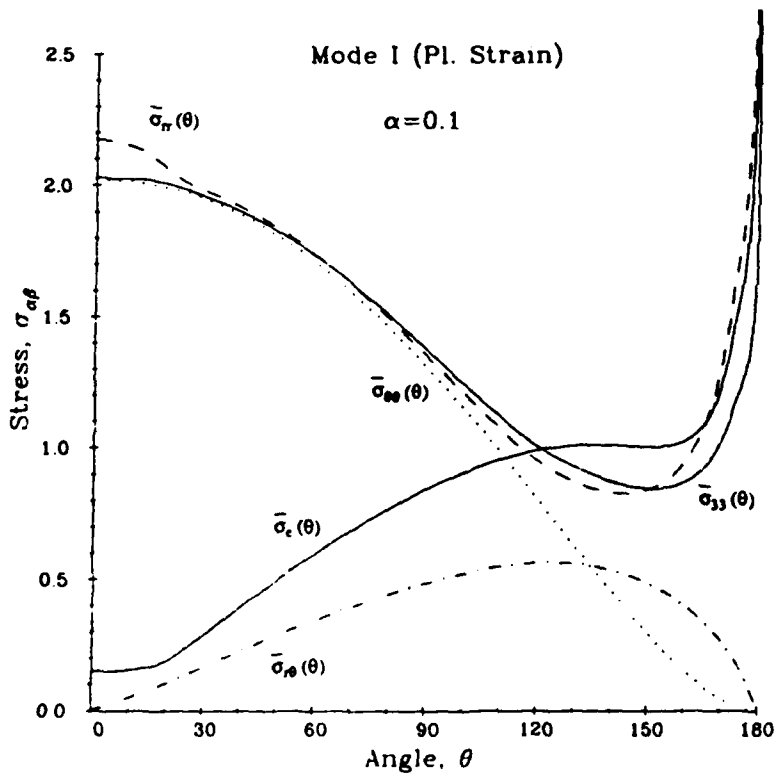

Figure 3.3b—Angular stress distribution in plane strain mode I for moderate strain-hardening, normalised such that $\bar{\sigma}_e(\theta_1) = 1$.

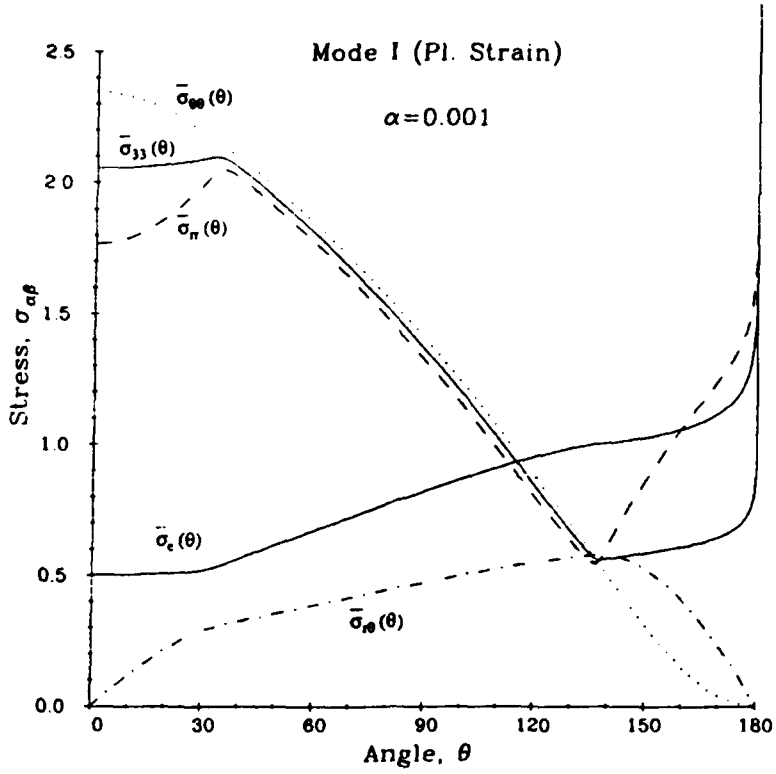

Figure 3.3c—Angular stress distribution in plane strain mode I for small strain-hardening, normalised such that $\bar{\sigma}_e(\theta_1) = 1$.

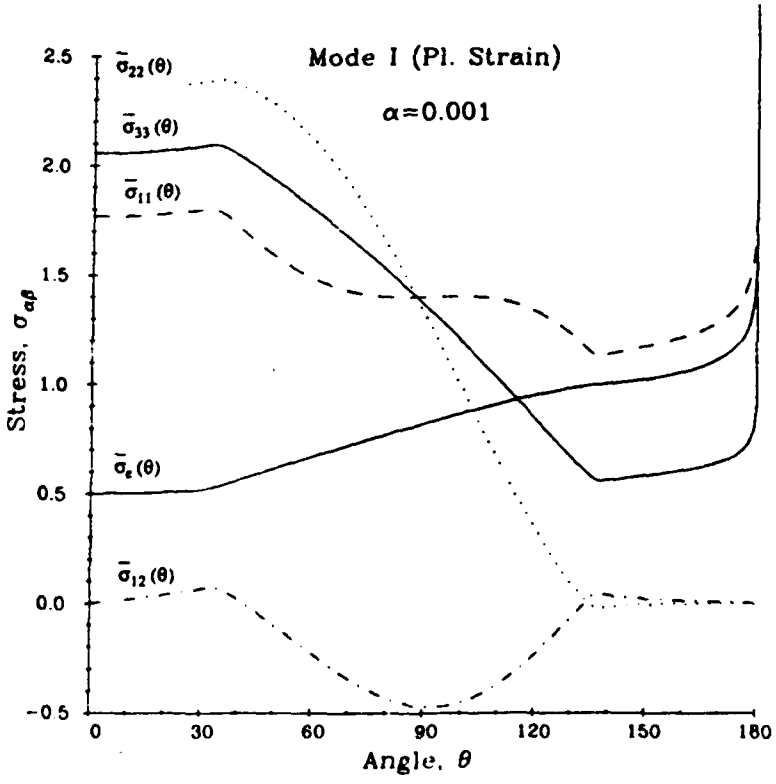

Figure 3.4—Angular stress distribution in plane strain mode I for small strain hardening, normalised such that $\bar{\sigma}_e(\theta_1) = 1$.

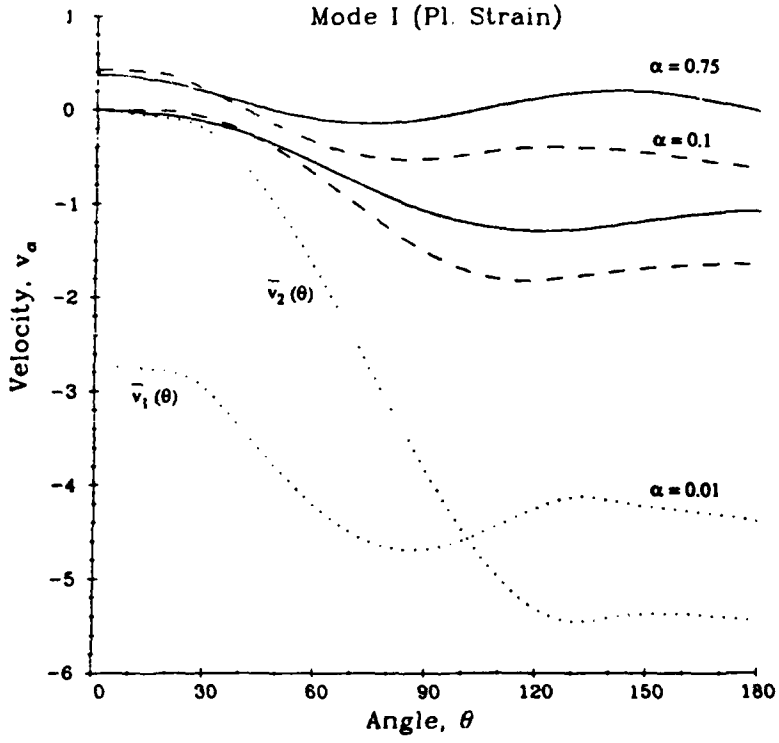

Figure 3.5—Angular velocity distribution in plane strain mode I for large, moderate, and small strain-hardening, normalised such that $\bar{\sigma}_e(\theta_1) = 1$.

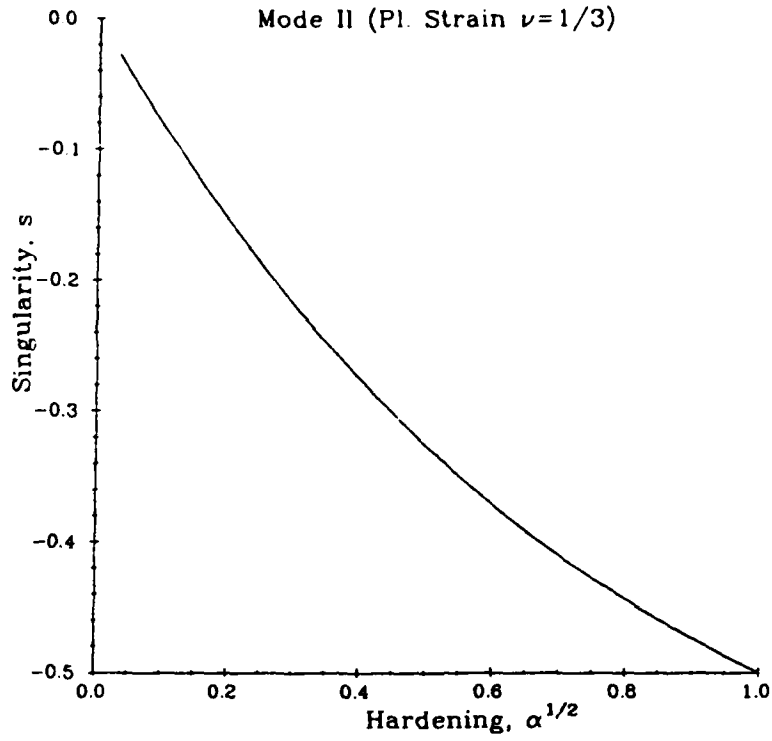

Figure 4.1—Strength of the singularity in plane strain mode II ($\nu = 1/3$).

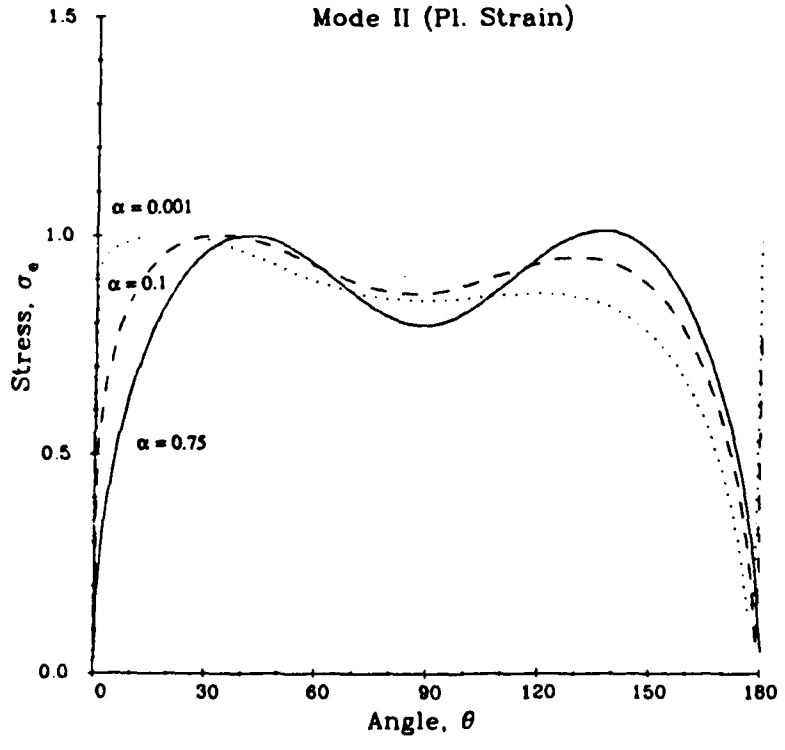

Figure 4.2—Particle effective stress distribution in plane strain mode II for large, moderate, and small strain-hardening, normalised such that $\sigma_e(r,\theta_1) = 1$.

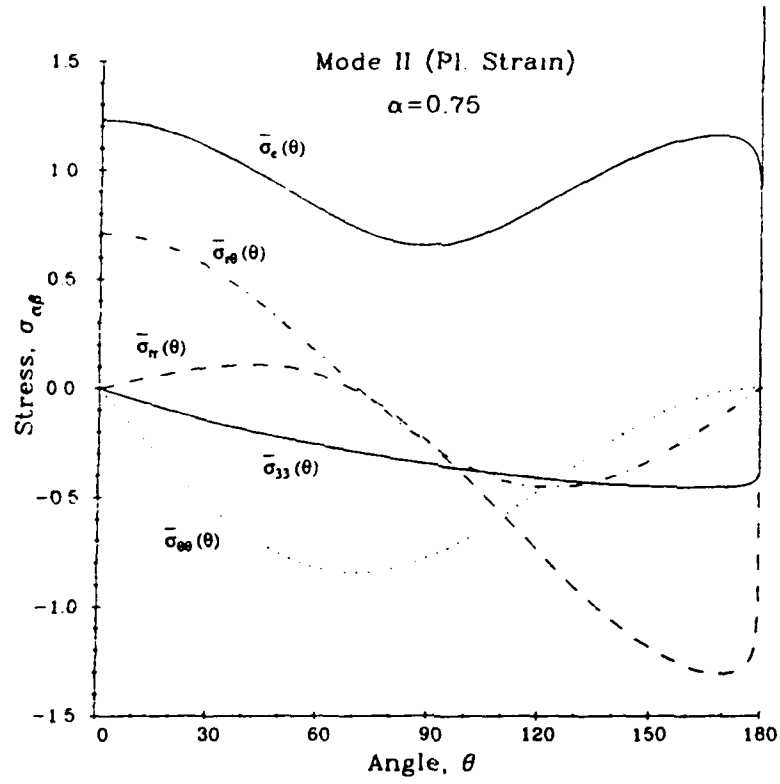

Figure 4.3a—Angular stress distribution in plane strain mode II for large strain-hardening, normalised such that $\bar{\sigma}_e(\theta_1) = 1$.

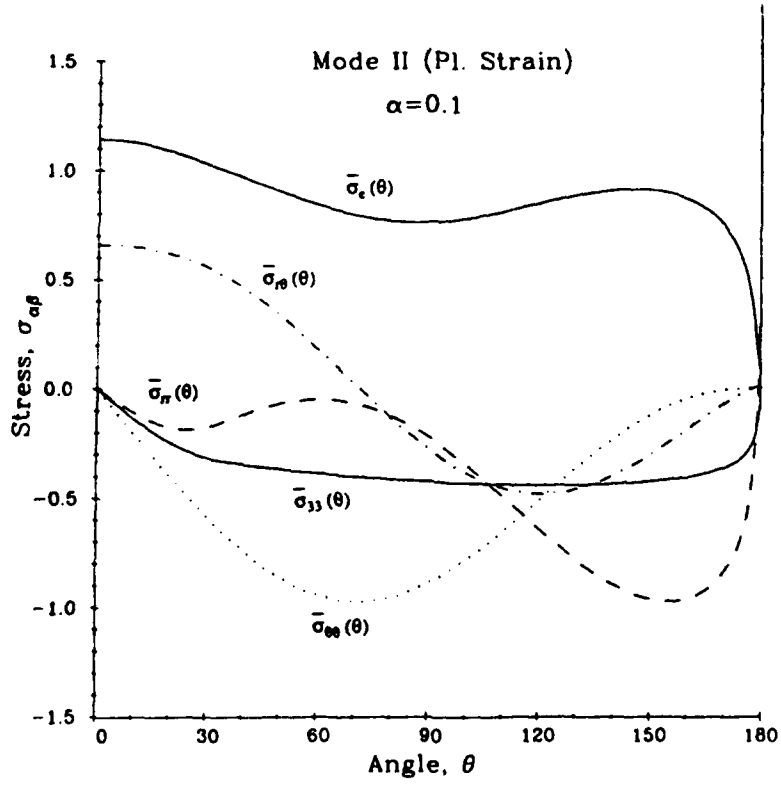

Figure 4.3b—Angular stress distribution in plane strain mode II for moderate strain-hardening, normalised such that $\bar{\sigma}_e(\theta_1) = 1$.

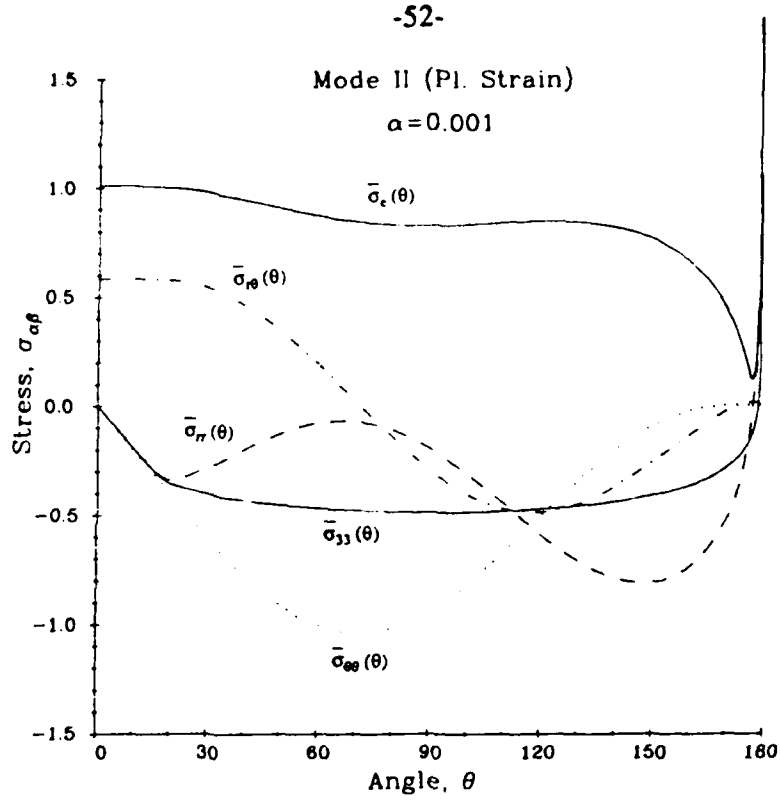

Figure 4.3c—Angular stress distribution in plane strain mode II for small strain-hardening, normalised such that $\bar{\sigma}_e(\theta_1) = 1$.

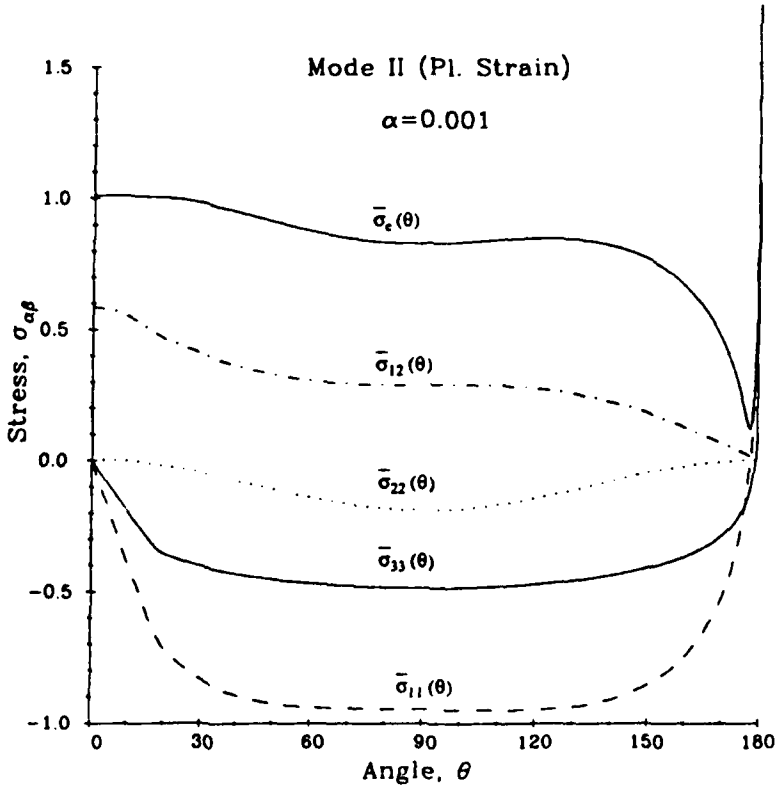

Figure 4.4—Angular stress distribution in plane strain mode II for small strain-hardening, normalised such that $\bar{\sigma}_e(\theta_1) = 1$.

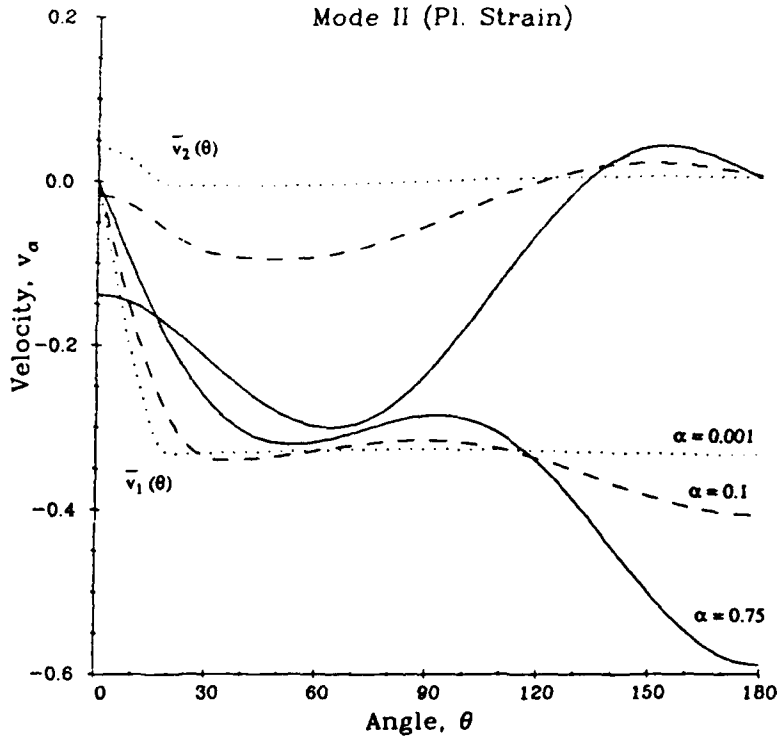

Figure 4.5—Angular velocity distribution in plane strain mode II for large, moderate, and small strain-hardening, normalised such that $\bar{\sigma}_e(\theta_1) = 1$.

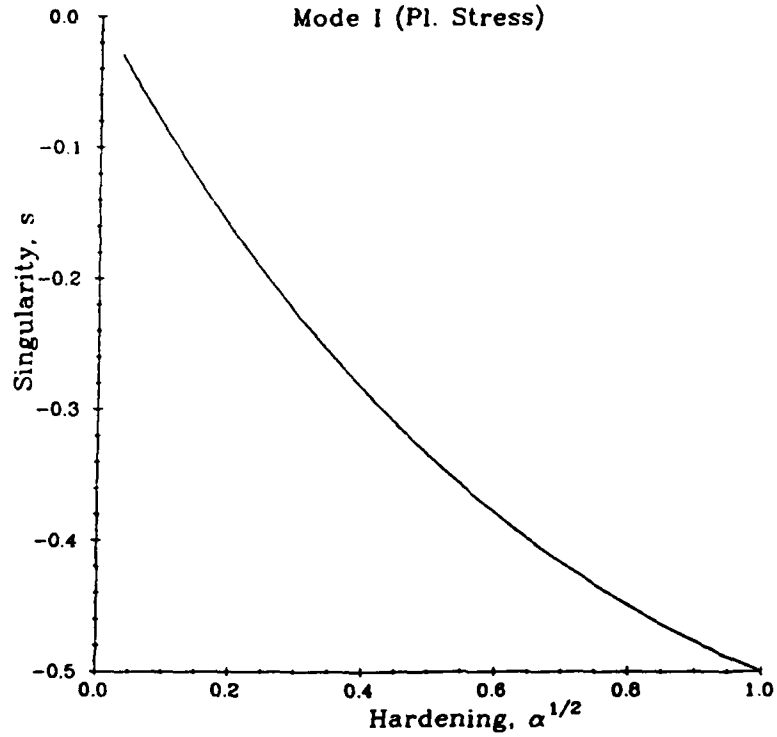

Figure 5.1—Strength of the singularity in plane stress mode I ($\nu = 1/2$).

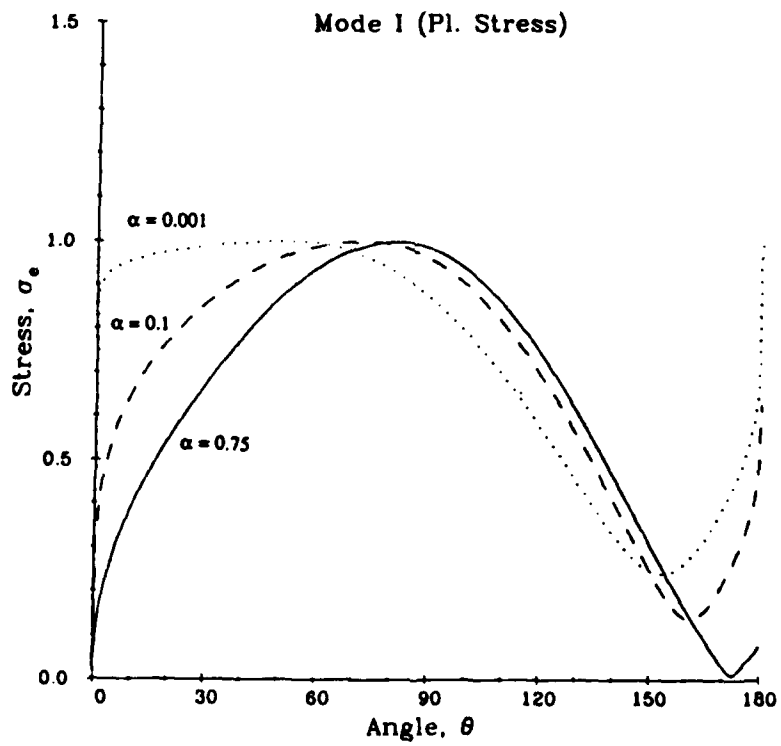

Figure 5.2—Particle effective stress distribution in plane stress mode I for large, moderate, and small strain-hardening, normalised such that $\sigma_e(r,\theta_1) = 1$.

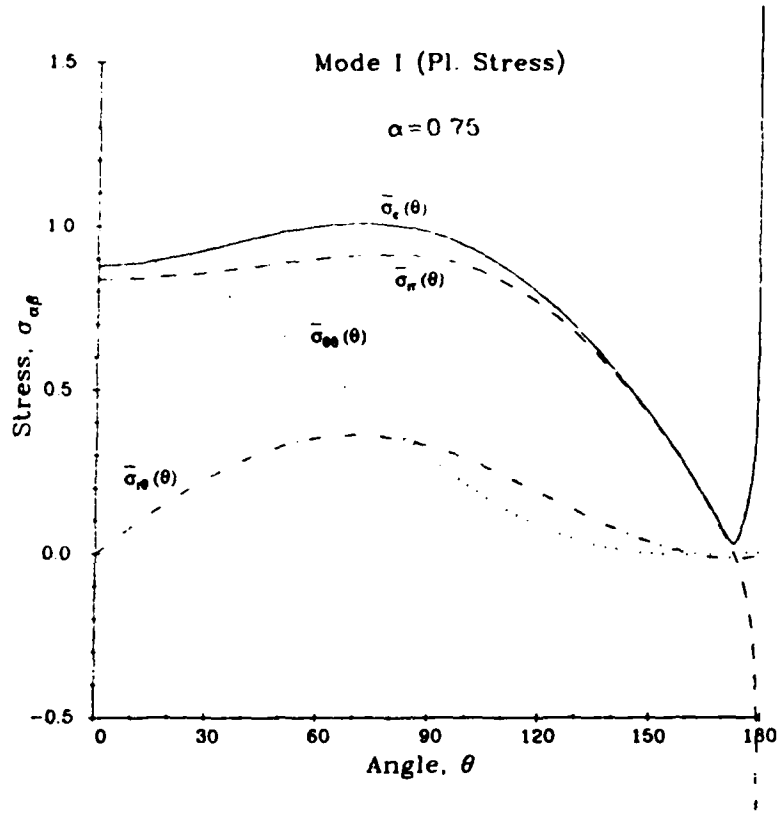

Figure 5.3a—Angular stress distribution in plane stress mode I for large strain-hardening, normalised such that $\bar{\sigma}_e(\theta_1) = 1$.

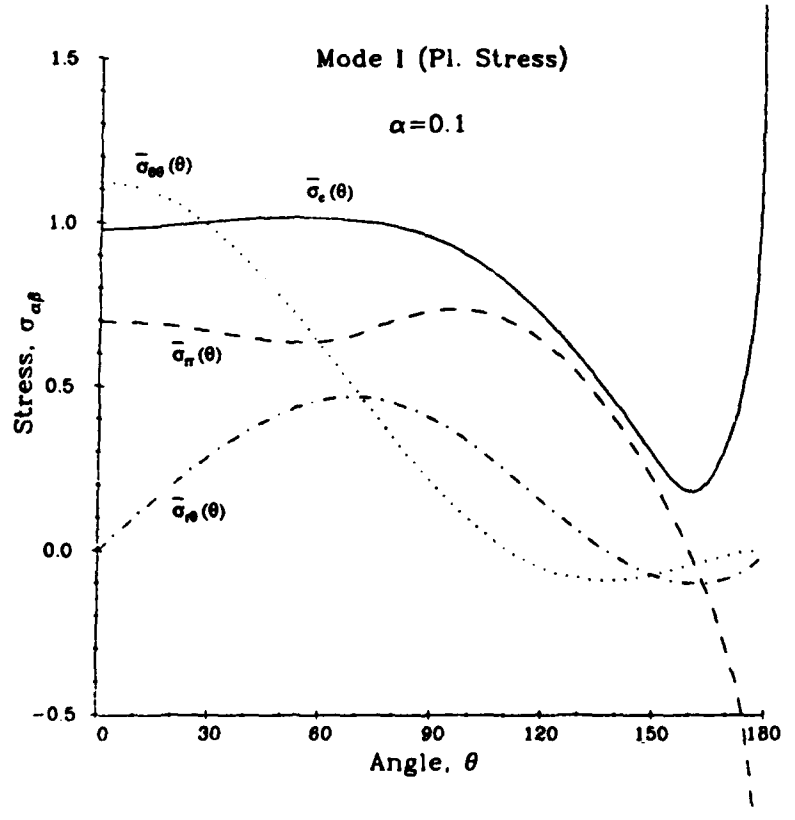

Figure 5.3b—Angular stress distribution in plane stress mode I for moderate strain-hardening, normalised such that $\bar{\sigma}_e(\theta_1) = 1$.

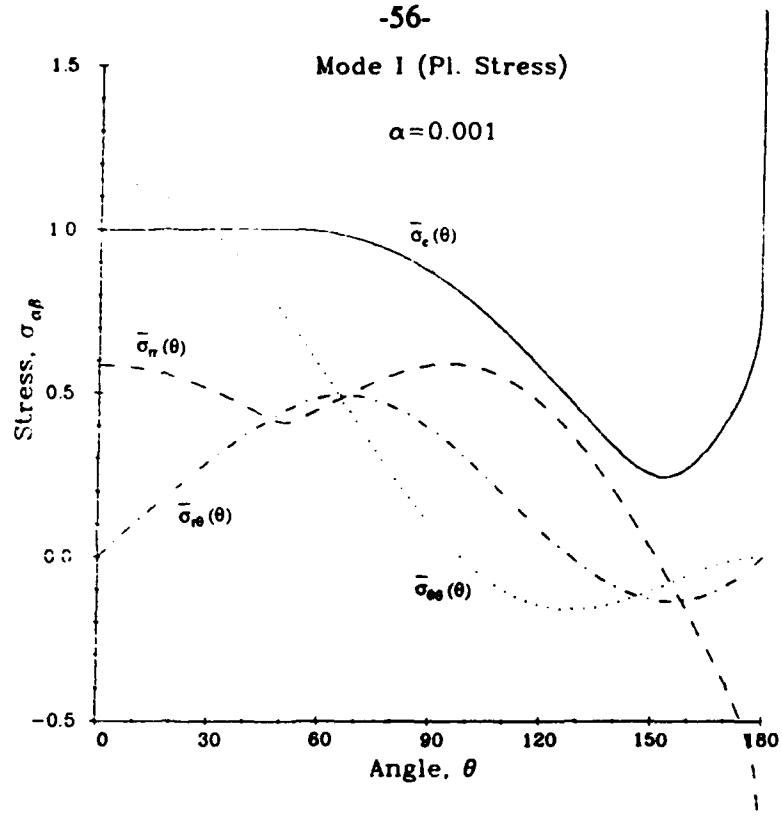

Figure 5.3c—Angular stress distribution in plane stress mode I for small strain-hardening, normalised such that $\bar{\sigma}_e(\theta_1) = 1$.

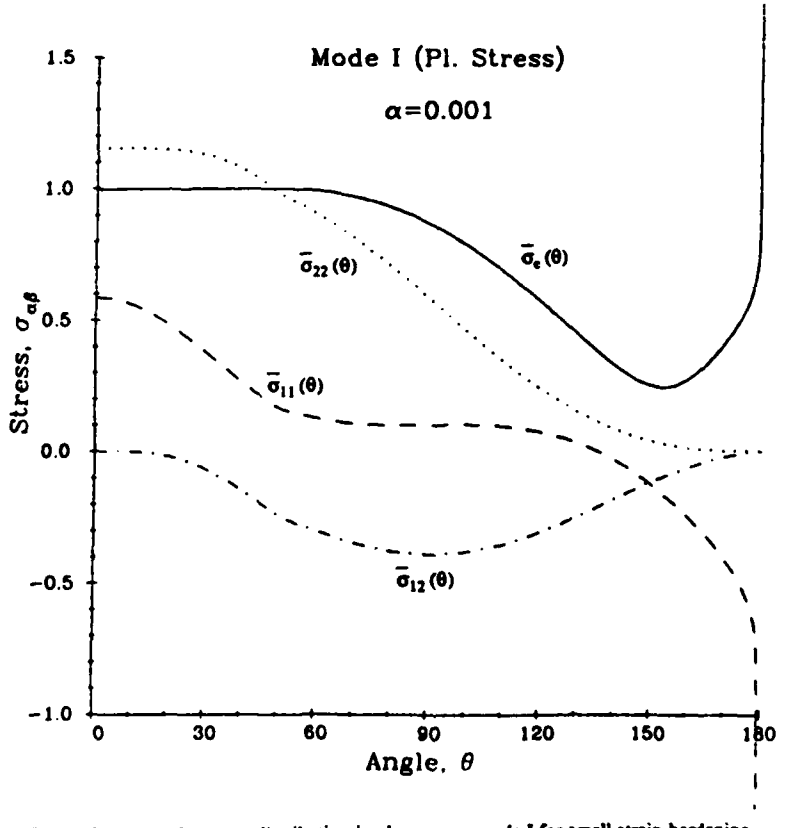

Figure 5.4—Angular stress distribution in plane stress mode I for small strain-hardening, normalised such that $\bar{\sigma}_e(\theta_1) = 1$.

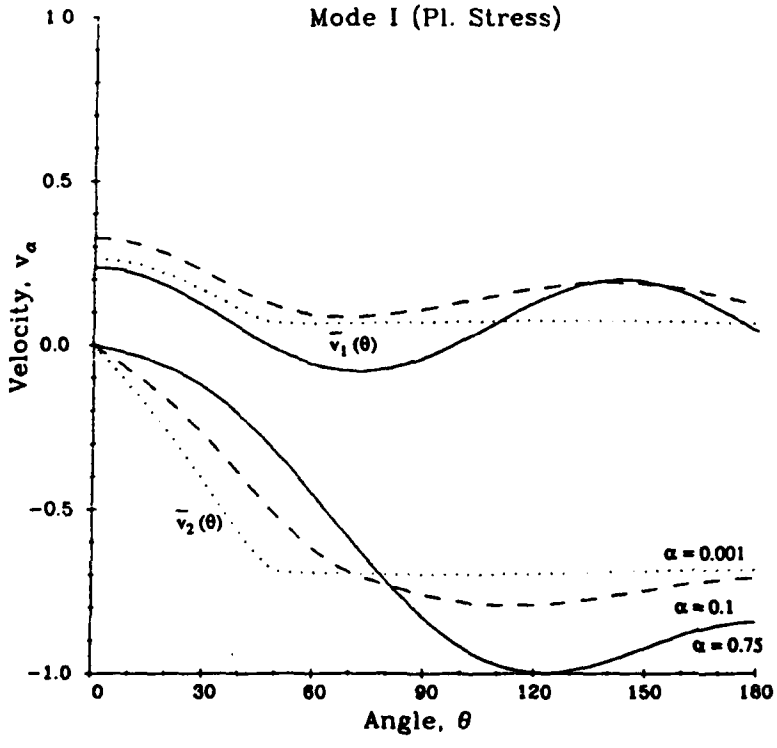

Figure 5.5—Angular velocity distribution in plane stress mode I for large, moderate, and small strain-hardening, normalised such that $\bar{\sigma}_e(\theta_1) = 1$.

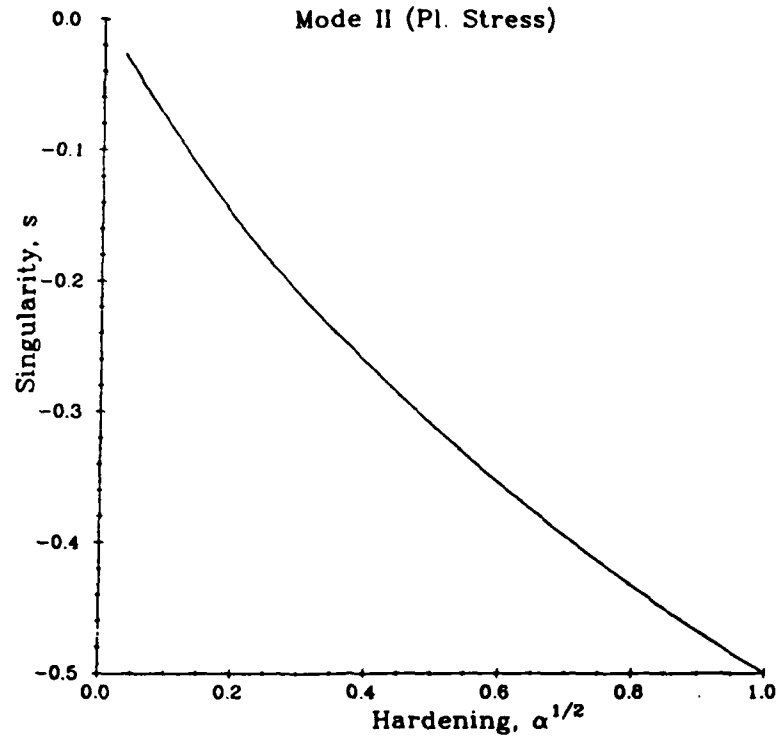

Figure 6.1—Strength of the singularity in plane stress mode II ($\nu = 1/2$).

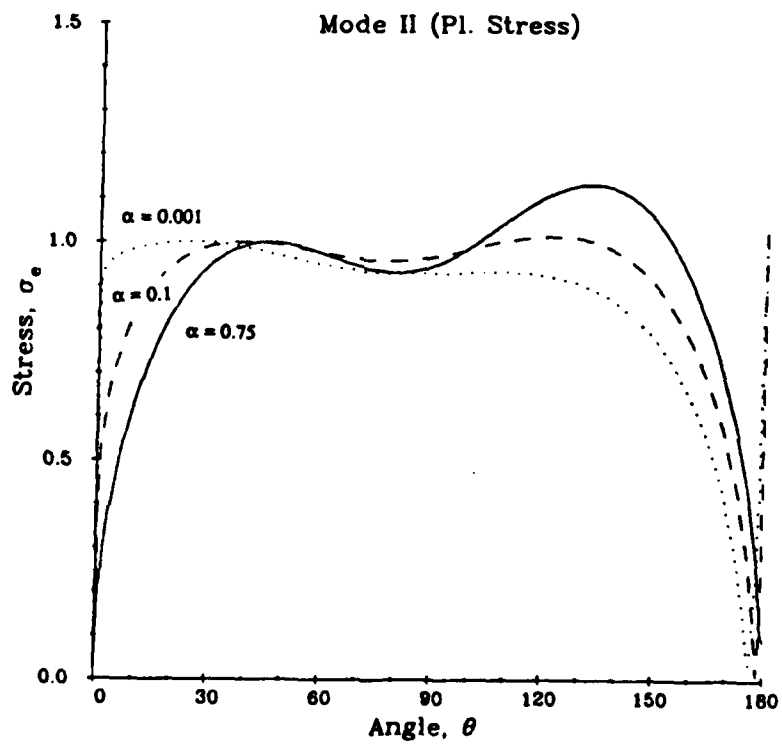

Figure 6.2—Particle effective stress distribution in plane stress mode II for large, moderate, and small strain-hardening, normalised such that $\sigma_e(r,\theta_1) = 1$.

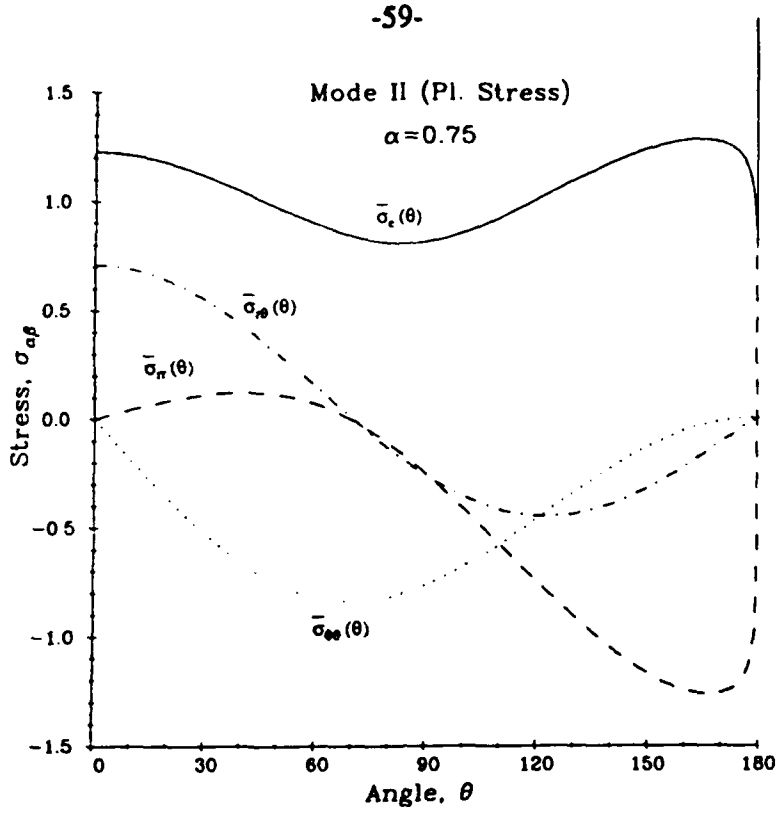

Figure 6.3a—Angular stress distribution in plane stress mode II for large strain-hardening, normalised such that $\bar{\sigma}_e(\theta_1) = 1$.

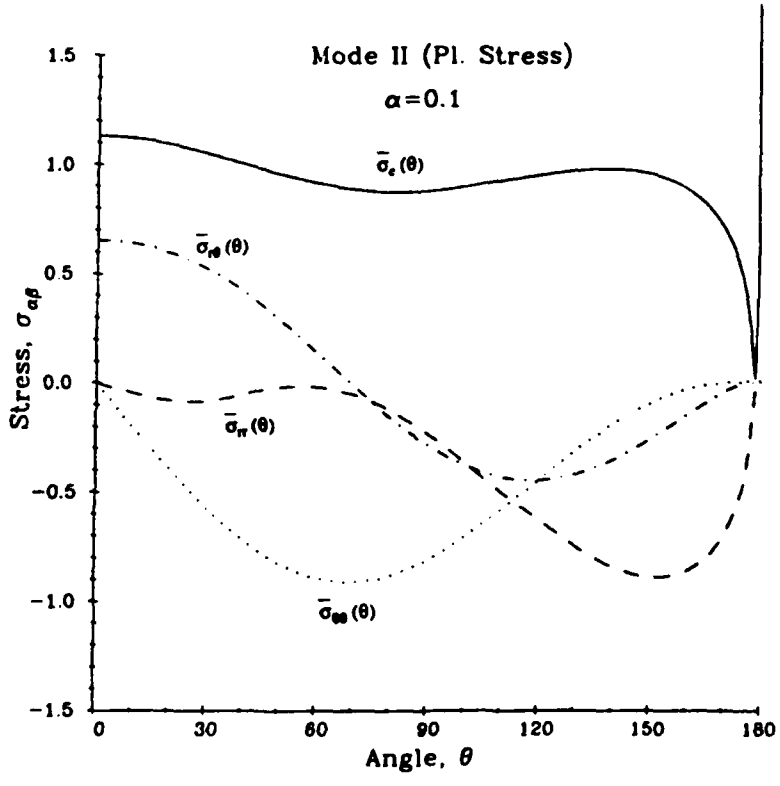

Figure 6.3b—Angular stress distribution in plane stress mode II for moderate strain-hardening, normalised such that $\bar{\sigma}_e(\theta_1) = 1$.

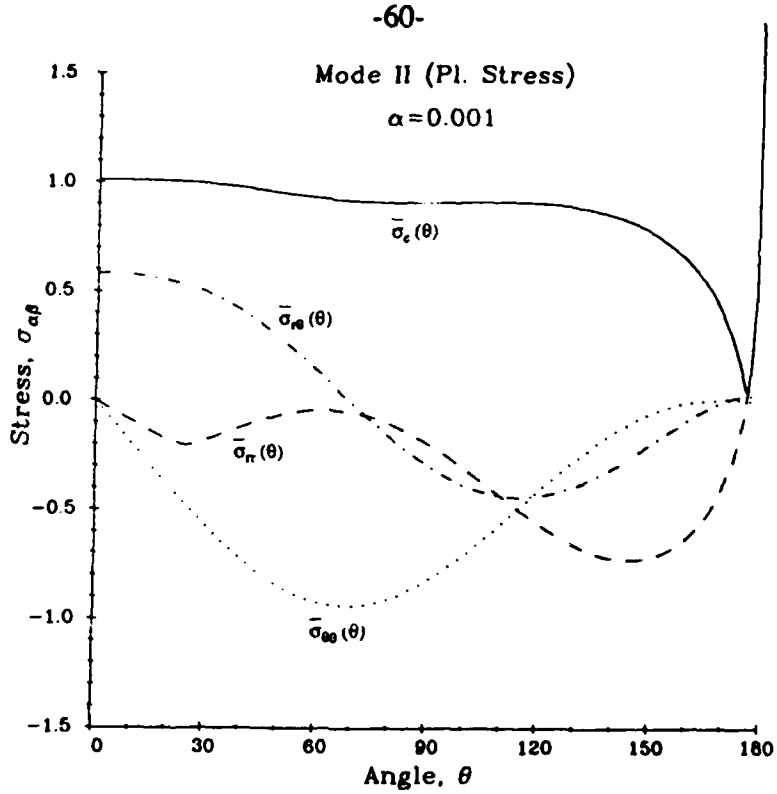

Figure 6.3c—Angular stress distribution in plane stress mode II for small strain-hardening, normalised such that $\bar{\sigma}_e(\theta_1) = 1$, normalised such that $\bar{\sigma}_e(\theta_1) = 1$.

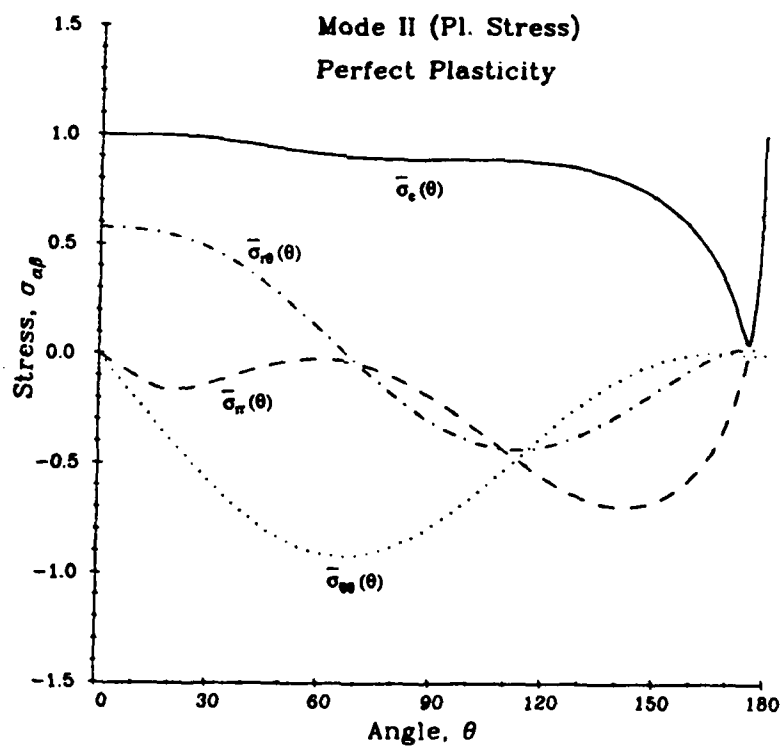

Figure 6.4—Angular stress distribution in plane stress mode II for perfect-plasticity, normalised such that $\sigma_o = 1$.

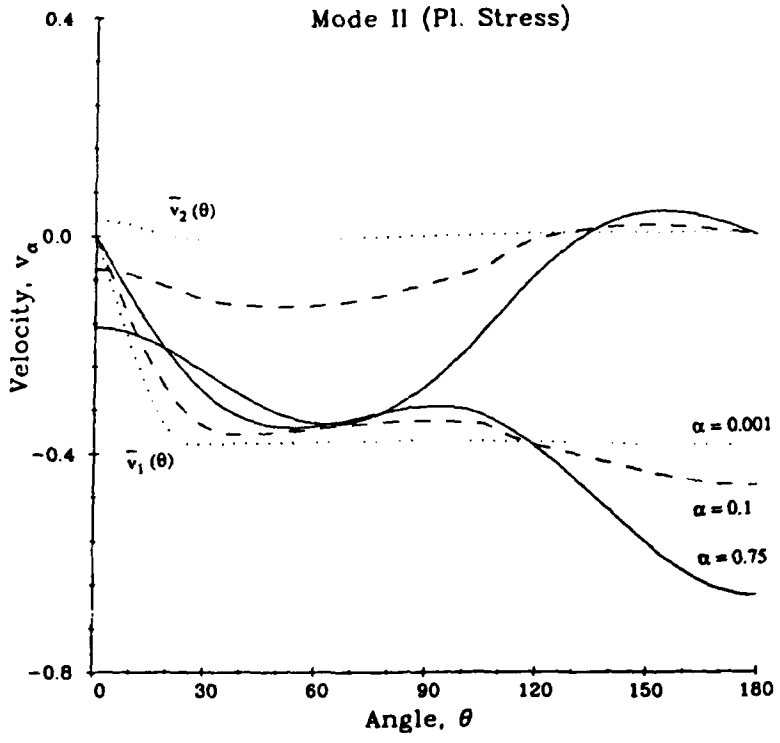

Figure 6.5—Angular velocity distribution in plane stress mode II for large, moderate, and small strain-hardening, normalised such that $\bar{\sigma}_e(\theta_1) = 1$.

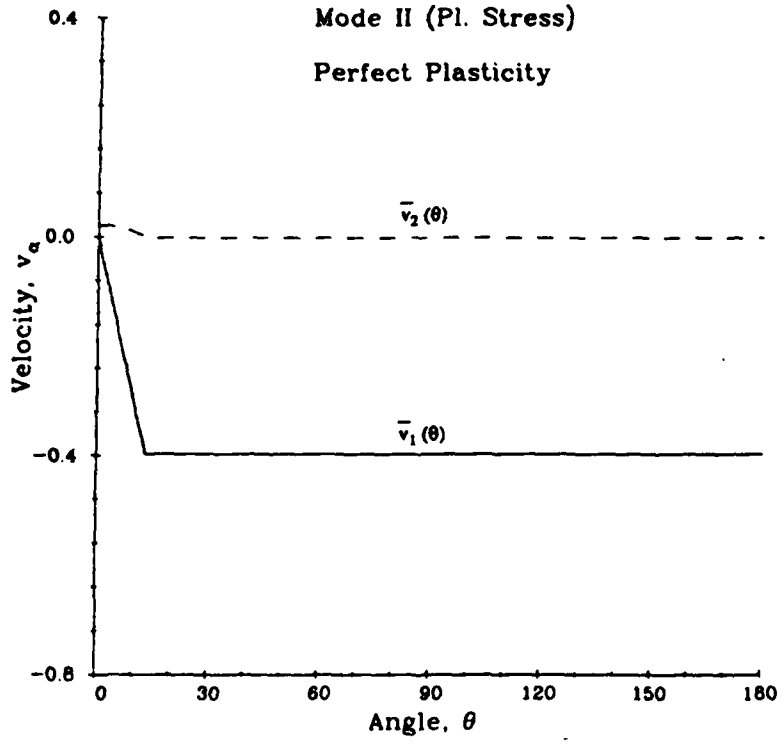

Figure 6.6—Angular velocity distribution in plane stress mode II for perfectly-plasticity, normalised such that $\sigma_o = 1$.

END

FILMED

12-85

DTIC